Faculteit der Technische natuurkunde van de T.U. Delft

Interfacial tension measurements using electrically generated spatially damped capillary waves

M.J. Colon

2e afstudeerverslag
Begeleiding T.U. Delft
Afstudeerdocent: Prof. J.M. Smith M.Sc
Mentor: Dr. Ir. M.M.C.G Warmoeskerken
Begeleiding SHELL (KSEPL Rijswijk)
Dr. P.B. van der Weg
Ir. A.M. Michels

Delft
8-10-1987

SUMMARY

The aim of this investigation was to evaluate a new technique to measure the dynamic interfacial parameters of an oil-water interface. This technique might eventually be used at resevoir conditions. The technique is based on the generation of waves at an interface. The propagation of these waves is monitored with an optical system. From the measured dispersion of those waves the interfacial parameters as interfacial tension or interfacial elasticity and viscosity can be evaluated.

The technique is tested in an experimental setup and two dedicated measurement cells are built to study an oil-water and a microemulsion system in more detail.

The experiments show that the technique is useful for interfacial tension measurements. An accuracy better than 1% can be reached. There are certain limitations to this technique:
- One of the phases must be non-conducting
- the phases must have an appreciable difference in permittivity.
- At least one of the phases must be transparant for light.

The wavelength of the propagating wave is used to measure the interfacial tension. The damping of the wave can be used to measure viscosity, accuracy however will be approximately 10% . Interfacial elasticity and viscosity are not calculated in this investigation. Measurements with microemulsion systems could not be done satisfactory. The interaction of the interface with the field is not as expected and further study is necessary to evaluate this.

With a measurement cell (diameter 2 cm) the miniaturisation needed for a pressurised vessel was investigated. Interfacial tension measurements showed to be well possible with this cell.

This investigation is carried out at the Royal/Dutch Shell Exploration and Production Laboratory (KSEPL) in Rijswijk; Under supervision of Dr P.B. van der Weg (Shell), Ir. A.M. Michels (Shell), Dr. Ir M.M.C.G. Warmoeskerken (TU Delft) and Prof. J.M. Smith M.Sc (TU Delft).

CONTENTS

1 Introduction.

Especially after rises in oil price enhanced oil recovery became of interest to the oil-industry. Enhanced oil recovery means producing more oil by using not just water as a fluid to displace oil from the reservoir, but adding small amounts of agents to improve the displacement efficiency of the fluid. Two important types of agents used are polymers,and surfactants. Polymers are used to increase viscosity,and surfactants are used to lower the oil/water interfacial tension. Detailed description of multiphase flow of oil and water in a reservoir (consisting of porous sediment) is very complicated, especially when agents are added. Many physical parameters are needed for the description of such a dynamic process and prediction of the efficiency of the recovery is even more complex. For the description of flow of interfaces the more important parameters are interfacial tension, interfacial elasticity and interfacial viscosity. These parameters should be measured at reservoir conditions, thus at elevated pressure (hundreds of bars) and elevated temperature (up to 200 degree Celsius).

The aim of this investigation was to evaluate a new technique to measure the dynamic interfacial parameters of an oil-water interface, that might eventually be used at resevoir conditions The technique is based on the generation of waves at an interface. From the measured dispersion of those waves the interfacial parameters as interfacial tension or interfacial elasticity and viscosity can be evaluated.

The technique is tested in an experimental setup. Design parameters are adapted to meet additional requirements like pressurisation and to improve the result. Theoretical description had to be extended to meet those requirements and tested with experiments.

2 Historical background

In literature many experimental techniques to measure interfacial/surface tension are mentioned:

1 pendent/sessile drop profile
2 capillary rise
3 bubble pressure
4 drop weight/volume/time
5 ring/plate removal
6 oscillating drop
7 spinning drop
8 capillary wave
9 plate/force

A detailed discussion will be given for the methods suited for dynamical measurements: plate/force and capillary wave.

Wilhelmy plate/force, is a method working with an interfacial trough in which a plate hangs in the interface while the interface is compressed by moving barriers. The force is measured with a balance, changes in the interfacial tension are measured during the changes in interfacial area. Until recently this method was operational at KSEPL under atmosferic conditions. The size and the operations of the equipment are responsible for two limitations of the system:

-Difficult to pressurise the cell.
-Time scales measurable this way range from 0.5 sec. and longer.

The capillary wave method is based on the dispersive behaviour of so called capillary waves at an interface. Theoretical work leads to a dispersion relation, linking fluid and interfacial parameters, to wave parameters. There are two ways to use this phenomenon:

- Light scattering by thermally induced capillary waves. The spectrum of this signal can be linked to the dispersion relation.(Ref.(1,2,3,4))

- Specular reflection of a small laser beam from electrically generated propagating capillary waves. The spatial attenuation and wavelength are measured and used to calculate interfacial parameters. The experiments mentioned in literature are mainly for plane waves (Ref(5,6,7,8,9).

Based on this literature the experiments started with a plane wave geometry. Later on radial waves were used and theory will be focused on them.

3 Theory and experimental background.

3.1 Introduction

The theoretical description can be devided in two areas, a physics part and a technical part.

The physical part will start with the interface itself, its behaviour and the relevant parameters. The next issue is the type, propagation, attentuation, and disperssion of waves at the interface. As an example a simplified form of dispersion relation is derived. A full treatment of wave dispersion is omitted. In literature there are extensive studies in this field (Ref(5,9,10,11,12). I will mention the main results.

In the technical part the theory concerning the experimental setup is described. The techniques to generate the different waves at an interface are explained. An expression is derived for the actual interaction between electrical field and interface to predict the waveform. Theory is developed to describe the wave detection and signal processing. Finally the resulting experimental configurations are described.

3.2 Theory

3.2.1 Interfacial phenomena

In real systems, there is a finite distance across an interface in which the properties gradually change from those of one adjacent bulk phase to those of the other. In literature two different models are used. In the approach of Guggenheim (1967) the interface is treated as a phase which is adjacent to the bulk phases and which has a finite thickness and volume. To calculate properties of an interface this way is still very dificult. Gibbs (1928) considered a more practical way to model an interfacial system.

The interface is regarded as a mathematical dividing plane (Gibbs surface). Surface excess parameters are defined with respect to that plane. In thermodynamics there are a few equivalent definitions of γ the interfacial tension, based on the internal energy U, the Gibbs free energy G or the Helmholz free energy H:

$$\gamma = \left(\frac{\partial U}{\partial A}\right)_{S,V} = \left(\frac{\partial G}{\partial A}\right)_{T,P} = \left(\frac{\partial H}{\partial A}\right)_{T,V} \qquad (1)$$

A is the interfacial area and S,T,P,V are the thermodynamic properties Entropy, Temperature, Pressure and Volume (Ref(14,15)) The dimension of γ in SI units [N/m], i.e. force per unit length, can also be seen as [J/m^2] which shows γ as energy per unit area. When γ changes with position, interfacial rheology comes into play. In a linearised theory (Ref(10,11,12,21,22)) four rheological parameters are defined:

- ϵ_s the interfacial shear elasticity.
- λ_s the interfacial dilatational elasticity.
- κ_s the interfacial dilatational viscosity.
- μ_s the interfacial shear viscosity.

3.2.2 waves

Wave theory is well developed. I will just mention the classifications relevant to this study.

- transversal versus longitudinal. In fig 1A the difference is explained.
- plane versus radial waves, see fig 1B. They differ in wave source geometry and description.
- dispersive versus non dispersive. When waves are dispersive the propagation properties depend on the frequency.

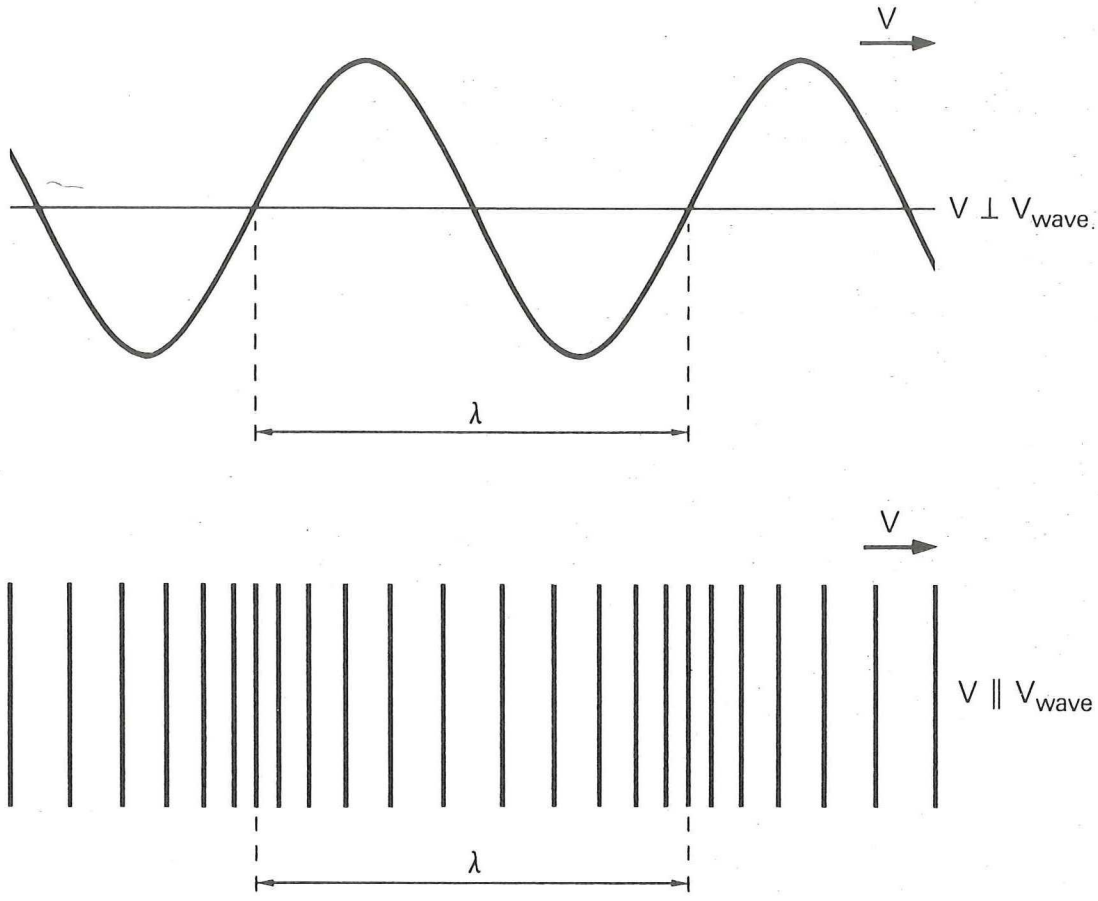

Fig. 1a The difference between transversal and longitudinal waves.

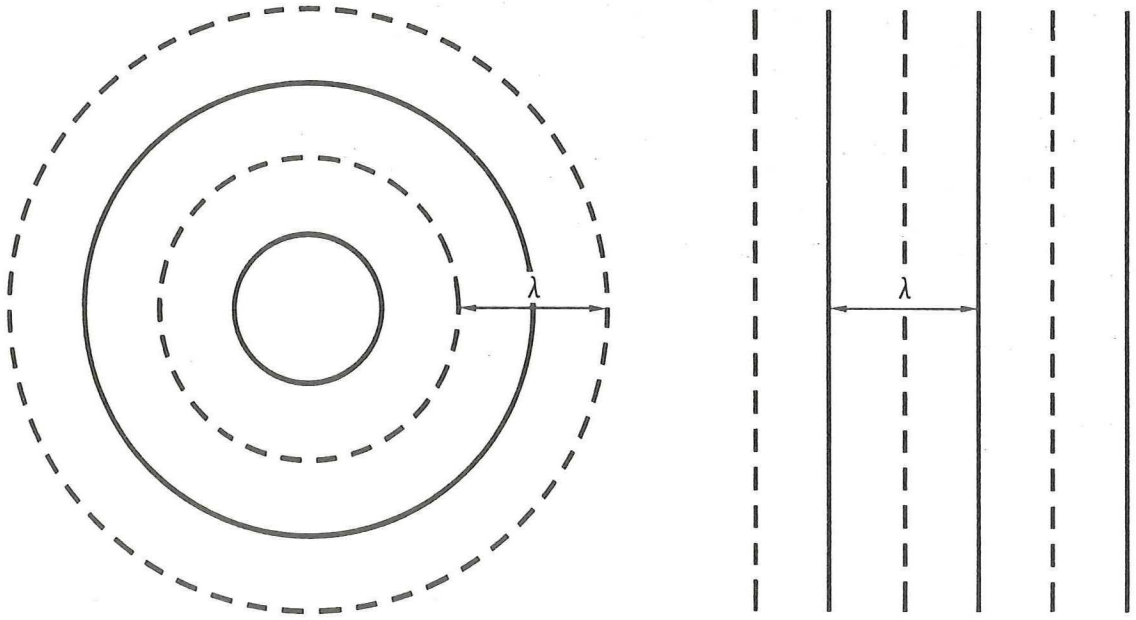

Fig. 1b The difference between plane and cylindrical waves.

3.2.3 Waves at interfaces.

Wave theory on fluids has a long history. Plinius the Elder mentioned already the calming effect of oil on water waves but he did not explain this phenomenon. In the 18th and 19th century physicists like Benjamin Franklin (1774), Lord Kelvin (1871) and Reynolds (1880) worked in this field. They developed the first mathematical description of the problem. Following Dorrestein (Ref(16,17)) a dispersion relation, this is a relation between k the wave number and ω the angular velocity will be derived. Plane waves, Newtonian fluid dynamics, a Cartesian coordinate system and special boundary conditions will be used.

The z-axis will be taken vertically upwards. The undisturbed interface of the fluids is postioned at z=0. The calculations are simplified by looking at a liquid-gas interface. Small velocities $\vec{V}$ are assumed so that terms quadratic in the velocities can be neglected. The following equations assuming plane waves ($\partial/\partial y=0$) are obtained:

$$\frac{\partial V_x}{\partial x} + \frac{\partial V_y}{\partial y} + \frac{\partial V_z}{\partial z} = 0 \qquad \text{continuity} \qquad (2)$$

$$\rho\frac{\partial \vec{V}}{\partial t} = -\frac{\partial p}{\partial x_i} + \eta\Delta\vec{V} + G_{x_i} \qquad \text{linearised Navier-Stokes equations} \qquad (3)$$

The non dissipative case i.e. $\eta=0$ is looked at. The boundary condition for the pressure at the interface $z=\xi$ is:

$$p_o - p = \gamma \frac{\partial^2 \xi}{\partial x^2} \quad (\text{ at the interface}) \qquad (4)$$

here $\sqrt{\{\ [1 + (\frac{\partial \xi}{\partial x})^2]^3\ \}}$

has been assumed to be close to 1, small $\frac{\partial \xi}{\partial x}$, so small amplitudes. A general solution is:

$$v_x = k\ D\ e^{kz} \cos(\omega t + kx) \qquad (5)$$

$$v_z = -k\ D\ e^{kz} \sin(\omega t + kx) \qquad (6)$$

$$p = p_o - \rho g z - \rho \omega\ D\ e^{kz} \cos(\omega t + kx) \qquad (7)$$

Combining the boundary condition [4] and eq [7] we find the dispersion equation, derived already by Lord Kelvin (23):

$$\omega^2 = gk + \frac{\gamma k^3}{\rho} \qquad (8)$$

At low values of k the $\gamma k^3/\rho$-term is small compared to gk. The wave shape is dominated by gravity effects, the so-called gravity waves. At high values of k the gravity term is small and the wave shape is dominated by interfacial tension effects, the so-called capillary ripples. The transition can be characterized by the quantity:

$$\frac{\gamma k^2}{\rho g}$$

If >> 1, the capillary forces win, << 1 gravity wins.

In the preceding derivation of this dispersion relation a few simplifications have been made. These simplifications can be removed, leading to a more involved dispersion relation:

1. A liquid-liquid interface instead of a liquid-gas interface.

This does not make the dispersion relation much more complicated, [8] becomes:

$$\omega^2 = \frac{\rho - \rho'}{\rho + \rho'} gk + \frac{\gamma k^3}{\rho + \rho'} \qquad (9)$$

where the prime indicates an upper phase parameter.

2. Liquids with a non-vanishing viscosity $\eta \neq 0$.

The viscosity makes fluid motion dissipative and thus leads to damping of wave motion. For spatially damped waves the wave number k is then complex:

$$k = m + i\alpha \qquad (10)$$

with real m and α.

$$V_x = (m + i\alpha)A\, e^{(m + i\alpha)z} \cos(\omega t + mx + i\alpha x) \qquad (11)$$

$$V_z = -(m + i\alpha)A\, e^{(m + i\alpha)z} \sin(\omega t + mx + i\alpha x) \qquad (12)$$

$$p = p_0 - \rho g z - \rho\omega A\, e^{(m + i\alpha)z} \cos(\omega t + mx + i\alpha x) \qquad (13)$$

The dispersion relation becomes a complex equation. The real part of the equation leads to the elementary dispersion relation [9]. The imaginary part gives the spatial damping, for capillary waves (ref.(5)):

$$\alpha = 4/3\, \frac{(\eta + \eta')\omega}{\gamma} \qquad (14)$$

It is necessary to keep in mind that this is a simplified equation, only true when the waves have small amplitudes and there is no elasticity and viscosity in the interface

3. Cylindrical waves

The equations of motion in cylindrical coordinates lead to a general solution based on Bessel functions instead of sinusoidals. When measurements are needed far from the source the following approximation for the zero order Bessel function J_0 can be used:

$$J_0(kr) \sim \frac{\cos(kr+\pi/4)}{\sqrt{(kr)}} \qquad (15)$$

The dispersion relation remains the same as for plane waves. For small kr the actual Bessel function must be used.

4. Interfacial rheology.

The linearised interface model, (§3.2.1) defines four extra parameters. If flux of material through or to the interface is important the created concentration gradients affect the value of γ and additional parameters are needed. To keep balance between theory and experiments, just the end result obtained by P.B. van der Weg (Ref(22)) will be given here.

We consider the attenuation and propagation of the interfacial wave at an interface far from the generator, the electrical term can then be neglected; (The electrical field goes to zero for high values of r). The equations for normal and tangential components of wave motion at the interface are two linear homogeneous equations in unknown coefficients $a(k,\omega)$ and $c(k,\omega)$. This set has non-trivial solutions only if the determinant $Det(k,\omega)$ of their coefficients is zero. This determinantal equation $Det(k,\omega)=0$ is the dispersion relation (9,10).

If ω is real we are looking at a steady state periodic solution for spatial propagation and attenuation at a free interface.

3.3 Experimental background

3.3.1 Introduction.

The experimental method is based on the measurement of the propagation of interfacial waves. By measuring wavelength and attenuation it is possible to calculate the parameters from the dispersion relation. The fluid parameters, density and viscosity are usualy known or easy to find. This leaves the interfacial parameters. An experimental setup is described, based on the setup used by Ting et al.(Ref(9)) fig 2.

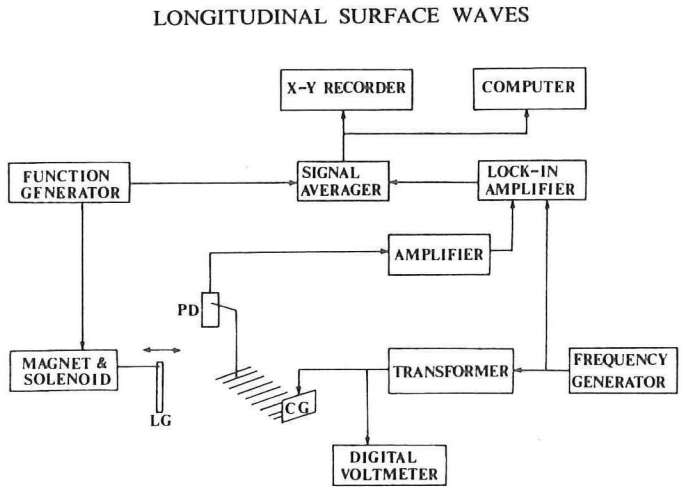

FIG. 5. Electronic diagram. CG: capillary wave generator, PD: position sensing photodiode, and LG: longitudinal wave generator.

Fig 2. The experimental setup used by Ting et al (Ref(9)).

There are three seperate parts; wave generation, wave detection and signal processing. All three will be looked at separately. In this investigation both plane and cylindrical waves are used.

3.3.2 Wave generation.

1. transversal waves.

Fluids rise into higher electric fields. This phenomenon can be used to generate local interface displacements and capillary waves between fluids of different electrical permittivity (Ref(18)). The fluid of the higher permittivity tends to accumulate at the higher electrical potential gradient. In this chapter a general model will be derived for wave generation. In a small vessel (as used in the measurement cells with cylindrical waves) the wave behaviour close to the electrode needs to be known. Detailed calculations will be made for the cylindrical case.

The energy of a horizontal homogeneous slab of liquid dielectric of permittivity ϵ_e' in a homogeneous vertical electric field is given by

$$U' = \frac{1}{2} \epsilon_e' \frac{A}{L} V_e^2 \qquad (16)$$

where L is a length in the direction of the field and A the perpendicular surface area and V_e the electrical potential difference over the dielectric. If we replace a small layer of liquid of thickness dz by a liquid with a higher permittivity ϵ_e , then the energy is

$$U = \frac{1}{2} A V_e^2 / [(1-dz)/\epsilon_e' + dz/\epsilon_e] \qquad (17)$$

The force f_e per unit area on a volume element of a substance with permittivity ϵ_e in another dielectric ϵ_e' trying to pull the volume element towards high potential (i.e. if $\epsilon_e > \epsilon_e'$) is

$$f_e^s = \frac{1}{A}\frac{dU}{dz} = \frac{U-U'}{A\,dz} \simeq \frac{1}{2}\,\epsilon_e'\,(\frac{V_e}{L})^2\,\frac{\epsilon_e - \epsilon_e'}{\epsilon_e} = \frac{1}{2}\,\epsilon_e'\,\frac{\epsilon_e - \epsilon_e'}{\epsilon_e}\,E^2 \quad (18)$$

The last equation shows that the force is proportional to the square of the potential gradient i.e. to the square of the local electric field strength[1] (19). For a given physical configuration the local force is proportional to the square of the total potential.
If the potential consists of the sum of a dc voltage V_{dc} and a sinusoidal ac voltage V_{ac} of frequency ω_e and if eq 16 holds for all these frequencies

$$V_e = V_{dc} + V_{ac} = V_{dc} + V_o\cos(\omega_e t) = V_{dc} + V_{ac}^{rms}\sqrt{2}\cos(\omega_e t) \quad (19)$$

the resulting force has stationary, first harmonic and second harmonic components. We know from eq.18 that the force exerted on the interface is proportional to the square of the instantaneous potential difference.

$$V_e^2 = [V_{dc}^2 + (V_{ac}^{rms})^2] + 2\sqrt{2}\,V_{ac}^{rms}V_{dc}\cos(\omega_e t) + (V_{ac}^{rms})^2\cos(2\omega_e t) \quad (20)$$

---

1. A more general equation for the force between two dielectrics with the field is not normal to the interface is given by

$$\vec{f}_e^s = (\epsilon_e - \epsilon_e')\,[\,E_t^2 + (\epsilon_e'/\epsilon_e)\,E_n^2\,]\,\vec{e}_n/2$$

where E_t is the field tangential and E_n the field normal to the interface.

So the stationary (total dc-) force is proportional to

$$(V_e^{rms})^2 = [V_{dc}^2 + (V_{ac}^{rms})^2] \qquad (21)$$

and harmonic force components are generated in both the first and second harmonic frequency. If $V_{dc} = 0$ then

$$V_e^2 = (V_{ac}^{rms})^2 + (V_{ac}^{rms})^2 \cos(2\omega_e t) \qquad (22)$$

and apart from the dc-component only the second harmonic component is generated. First we want to calculate the local force in an idealised electric field configuration. This model is not very realistic but already gives useful expressions. In the model we adjust a sphere (radius $R_0 <<$ millimeter) with electrical charge Q at r=0 in the upper phase a small distance h (a fraction of a millimeter, $h > R_0$) above the lower phase see figure 3a. The lower phase has a high permittivity and is grounded electrically. For the calculation of the field, we assume that the permittivity contrast between upper and lower phase is strong enough to produce a field only in the upper phase and that the upper phase is non-conducting. Consequently the field lines are perpendicular to the interface[2]. Because of the small distance of the charge to the interface, the field is strongly localised under the charge, giving only a localised electrical force pulling the interface upwards. The field between the charge and the interface is equal to the field in a hypothetical system of a point charge

---

2. At a less pronounced permittivity contrast the field extends in the lower phase and the field lines are broken at the interface:
$\tan(a') = (\epsilon_e'/\epsilon_e)\tan(a)$
where a' and a the angles in the upper and lower phase.

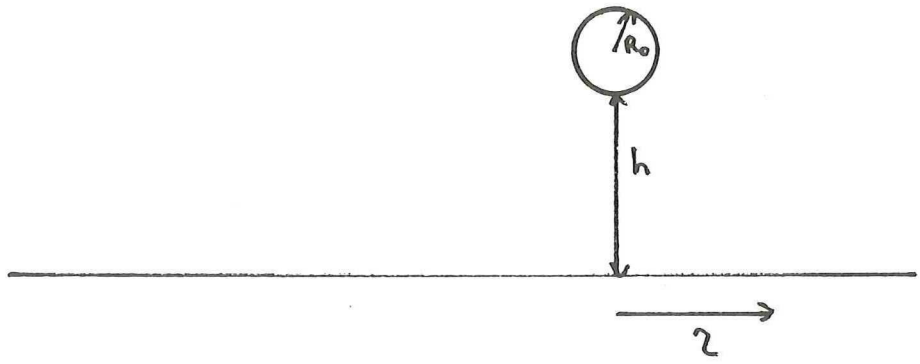

Fig. 3a. Model characteristics p.16.

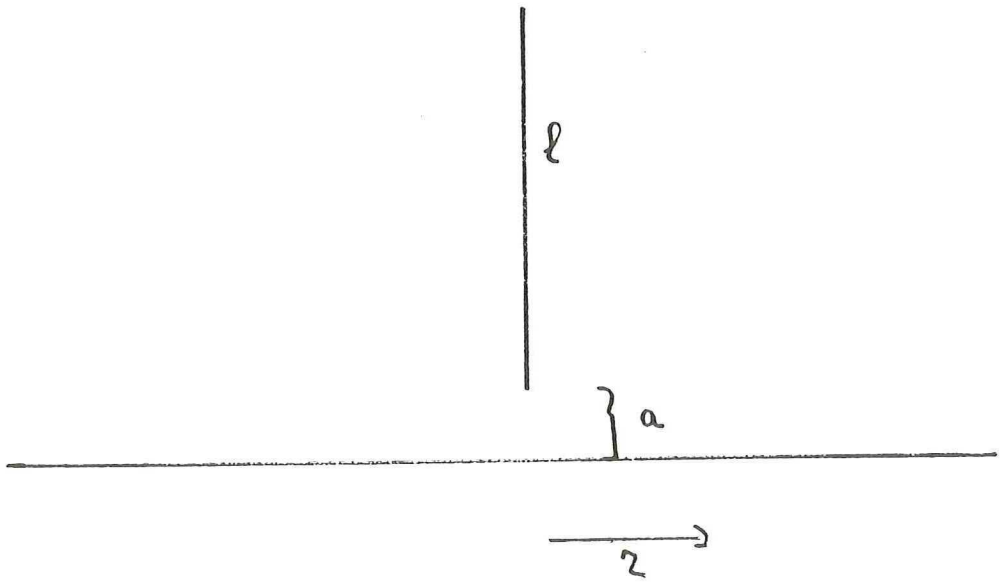

Fig.3b. Model characteristics p.19.

Fig 3a,b

and a opposite charged imaginary point charge at the same distance at the other side of the interface in a hypothetical dielectric of the same permittivity (Thomson or mirror image.) The potential from the charge and its image is at a point (z,r)

$$V = \frac{Q}{4\pi\epsilon'_e} \left[\frac{1}{\sqrt{[r^2+(h-z)^2]}} - \frac{1}{\sqrt{[r^2+(h+z)^2]}} \right] \qquad (23)$$

The field $\vec{E} = -\vec{\nabla}V$ is given by

$$\vec{E} = \frac{Q}{4\pi\epsilon'_e} \left[\frac{r}{\sqrt{[r^2+(h-z)^2]^3}} - \frac{r}{\sqrt{[r^2+(h+z)^2]^3}} \right] \vec{e}_r +$$

$$+ \frac{Q}{4\pi\epsilon'_e} \left[-\frac{(h-z)}{\sqrt{[r^2+(h-z)^2]^3}} - \frac{(h+z)}{\sqrt{[r^2+(h+z)^2]^3}} \right] \vec{e}_z \qquad (24)$$

The field at the interface is

$$\vec{E}(z=0) = \frac{-2Q}{4\pi\epsilon'_e} \frac{h}{[\sqrt{(r^2+h^2)^3}]} \vec{e}_z \qquad (25)$$

The potential at the surface of the charge is given by

$$V_e \simeq \frac{Q}{4\pi\epsilon'_e R_o} \qquad (26)$$

Inserting 25 and 26 into 18 gives for the force:

$$\vec{f}^s_e \simeq \frac{1}{2} \epsilon'_e \frac{\epsilon_e - \epsilon'_e}{\epsilon_e} \left[\frac{2Q}{4\pi\epsilon'_e} \right]^2 \frac{h^2}{[(r^2+h^2)^3]} \vec{e}_z \simeq$$

$$\simeq \frac{1}{2} \epsilon'_e \frac{\epsilon_e - \epsilon'_e}{\epsilon_e} V_e^2 \frac{4h^2R_o^2}{[(r^2+h^2)^3]} \vec{e}_z \qquad (27)$$

In this idealised configuration the expression for the force is already very complicated. As a better approximation we want to calculate the local force for a configuration more like the one used in our experiments. In the experiments we did use a vertical needle electrode sharpened towards its tip (total top opening angle ≃17 degrees) a distance h above the interface. To approximate its field we start with the field around a line charge of length ℓ vertically at r=0 in the upper phase a small distance a (a fraction of a millimeter) above the lower phase (See fig. 3b). The charge on the line per vertical unit of length ρ_e is assumed to be constant. The lower phase has a higher permittivity and is grounded electrically. We may take any equipotential plane around the uniformly charged line as the surface of a cylinder electrode. If ℓ is large, the shape of such an electrode is almost equivalent with the cone-like needle, sharpened towards its tip, increasing the actual charge density at the tip[3]. For the calculation of the field, we assume that the permittivity contrast between upper and lower phase is strong enough to produce a field only in the upper phase and consequently that the field lines are perpendicular to the interface. Because of the small distance of the line charge to the interface, the field is strongly localised under the line, giving only a localised electrical force pulling the interface upwards. The field between the line and the (idealised conducting) interface is equal to the field in a hypothetical system of the line and a mirror image of the dielectric and line in the interface (Thomson or mirror image.)

---

3. From the formula of the self-capacity of a spherical charge $Q_e = CV = 4\pi\epsilon'_e R_0 V_e$, where ϵ'_e is the permittivity of the medium and R_0 the radius, we may see $\rho_e = Q_e/4\pi R_0^2 = \epsilon'_e V_e/R_0$. This is an example to show that the charge density of a curved metal surface is proporional to its total curvature $(R_1^{-1}+R_2^{-1})$.

The charge on the mirror line is opposite to the charge on the line. The field from a small element dz of the line is at the interface (z=0)

$$d\vec{E} = \frac{\rho_e dz}{4\pi\epsilon'_e R^2}\vec{e}_R \qquad (28)$$

where $\vec{e}_R$ is the unit vector in the direction of the vector $\vec{R}$, the vector from the element dz to the interface. The contribution to the field in vertical direction is

$$dE_z = \frac{\rho_e dz}{4\pi\epsilon'_e R^2}(\vec{e}_R \cdot \vec{e}_z) = \frac{\rho_e z\ dz}{4\pi\epsilon'_e R^3} \qquad (29)$$

The mirror image (at -z) gives an identical vertical contribution. The horizontal contribution of the mirror is opposite: the horizontal component vanishes. The total (vertical) field at the interface is

$$\vec{E}(z=0) = \vec{e}_z \int_a^{\ell+a} \frac{2\rho_e z\ dz}{4\pi\epsilon'_e R^3} = \vec{e}_z \int_a^{\ell+a} \frac{2\rho_e z\ \ dz}{4\pi\epsilon'_e [\sqrt{(r^2+z^2)}]^3} =$$

$$= \frac{2\rho_e}{4\pi\epsilon'_e}\left[\frac{1}{[\sqrt{(r^2+a^2)}]} - \frac{1}{[\sqrt{(r^2+(a+\ell)^2)}]}\right]\vec{e}_z \qquad (30)$$

We now assume $r \ll \ell$ and $a \ll \ell$, then

$$\vec{E}(z=0) \simeq \frac{2\rho_e}{4\pi\epsilon'_e}\frac{1}{[\sqrt{(r^2+a^2)}]}\vec{e}_z \qquad (31)$$

The force is then given by

$$\vec{f}^{s}_{e} \simeq \frac{1}{2}\,\epsilon'_{e}\,\frac{\epsilon_{e}-\epsilon'_{e}}{\epsilon_{e}}\,\left[\frac{2\rho_{e}}{4\pi\epsilon'_{e}}\right]^{2}\frac{1}{(r^{2}+a^{2})}\,\vec{e}_{z} \qquad (32)$$

The potential of the line can be approximated by (Ref(20))

$$V_{e} = \frac{2\,\rho_{e}}{4\pi\epsilon'_{e}}\,\ln\left[\frac{2\ell}{d}\,\sqrt{\frac{(4a+\ell)}{(4a+3\ell)}}\right] \simeq \frac{2\,\rho_{e}}{4\pi\epsilon'_{e}}\,\ln\frac{2\ell}{d\sqrt{3}} \qquad (33)$$

Then

$$\vec{f}^{s}_{e} \simeq \frac{1}{2}\,\epsilon'_{e}\,\frac{\epsilon_{e}-\epsilon'_{e}}{\epsilon_{e}}\,\frac{V_{e}^{2}}{\ln^{2}\frac{2\ell}{d\sqrt{3}}}\,\frac{1}{(r^{2}+a^{2})}\,\vec{e}_{z} \qquad (34)$$

A still better approximation can be found by calculation of the electrical potential

$$V(r,z) = \frac{\rho_{e}}{4\pi\epsilon'_{e}}\int_{a}^{b}\{1/\sqrt{[(u-z)^{2}+r^{2}]}-1/\sqrt{[(u+z)^{2}+r^{2}]}\}du =$$

$$= \frac{\rho_{e}}{4\pi\epsilon'_{e}}\,\ln\left\{\frac{\sqrt{[(b-z)^{2}+r^{2}]}+(b-z)}{\sqrt{[(b+z)^{2}+r^{2}]}+(b+z)}\,\frac{\sqrt{[(a+z)^{2}+r^{2}]}+(a+z)}{\sqrt{[(a-z)^{2}+r^{2}]}+(a-z)}\right\} \qquad (35)$$

where b is the highest point of the line. If we assume $b\to\infty$ then

$$V(r,z) = \frac{\rho_{e}}{4\pi\epsilon'_{e}}\,\ln\frac{\sqrt{[(a+z)^{2}+r^{2}]}+(a+z)}{\sqrt{[(a-z)^{2}+r^{2}]}+(a-z)} \qquad (38)$$

Suppose $z=wr$ where w is a constant, and $r,z \gg a$ then

$$V(r,z) \to \frac{\rho_{e}}{4\pi\epsilon'_{e}}\,\ln\frac{\sqrt{(w^{2}+1)}+w}{\sqrt{(w^{2}+1)}-w} = V_{e} \qquad (37)$$

The potential curve approach a constant value V_{e} along $z=wr$.

This means that the potential curves behave at large values of z like straight lines: the shape is a sharpened needle. The constant w is for our experiments w = 6.70 for a top angle of 17 degrees. Suppose we select this equipotential as our electrode: V_e is then the potential on the electrode. The actual height h of the tip above the interface can be calculated by equating V(0,h) to V_e

$$V(0,h) = \frac{\rho_e}{4\pi\epsilon'_e} \ln \frac{a+h}{a-h} = V_e \qquad (38)$$

By comparing last two equations we find

$$a = (h/w) \sqrt{(w^2+1)} \qquad (39)$$

If we measure the actual height of the electrode h and the constant w (via the top angle of the cone) we may calculate the equivalent height a of a line charge, and thus characterise the entire field.
Then from eq 32 and eq 38

$$\vec{f}^{s}_{e} \simeq \frac{1}{2} \epsilon'_e \frac{\epsilon_e - \epsilon'_e}{\epsilon_e} \frac{V_e^2}{\ln^2 \frac{a+h}{a-h}} \frac{1}{(r^2+a^2)} \vec{e}_z \qquad (40)$$

We assume a sinusoidal potential

$$V_e = V_{ac}^{rms} \sqrt{2} \cos(\omega_e t) \qquad (41)$$

then

$$\vec{f}^{s}_{e} \simeq \beta_e \frac{1}{(r^2+a^2)} [1+\cos(2\omega_e t)] \vec{e}_z \qquad (42)$$

where β_e is given by

$$\beta_e = \frac{1}{2}\,\epsilon'_e\,\frac{\epsilon_e - \epsilon'_e}{\epsilon_e}\,\frac{(V_{ac}^{rms})^2}{\ln^2 \frac{a+h}{a-h}} \qquad (43)$$

In this case we have assumed that the shape of the needle electrode is like the equipotential plane around an infinitely long uniformly charged vertical line charge at a height a above the interface and looks like a sharp, infinitely long cylindrical cone. Around the tip the cone is rounded.

We conclude that the force is indeed proportional to $(V_{ac}^{rms})^2$ and is localised to a region $|r| < a$, rapidly ($\sim 1/r^2$) diminishing for $r > a$.

2. longitudinal waves

A loudspeaker is used as a wave generator. The cone of the loudspeaker is connected with a thin wire in the interface. The wire is acting as a moving barrier generating longitudinal waves. In practice this way of wave generation is limited in amplitude and frequency. Both high amplitudes and frequencies give rise to wave distortion and unwanted transversal waves.

3.3.3 Wave detection.

A laser beam is focussed on the interface. The incident wave can be perpendicular to the interface or at a grazing angle as sketched in figures 4 and 5. The beam is reflected at the interface which behaves like a mirror. The direction of the reflected beam contains information about the interface angle at the point of reflection. If a wave is present at the interface the direction of the reflected beam is modulated. A position sensing photo diode is used to detect the position of the reflected beam. This detector gives a voltage proportional to the position of a laser spot on its surface. Because the detector shows alinearity depending on the position of the spot at the detector surface a servo system is used to keep the average position of the spot at the middle of the detector. This servo system uses the dc component of the signal to move the detector. The ac component gives the information about the travelling wave. With a spectrum analyzer the spectrum of the signal can be recorded. In combination with the generator signal a lock-in amplifier selects the proper ac signals. The output of the lock-in amplifier consists of three components:
a) The magnitude of the detector signal in a small frequency domain.
b) A decomposition of this vector signal, in two circular components relative to the reference signal.
With a recorder plots of these signals can be made.

3.3.4 Signal processing.

The wave information must be deduced from the detector signal measured as a function of position of the laserspot at the interface. The laser beam will be followed to calculate the signal transfer. For grazing and perpendicular incident angles different results arise. The performance of the lock-in amplifier will be dealt with separately. The principles will be given for a perpendicular incident beam.

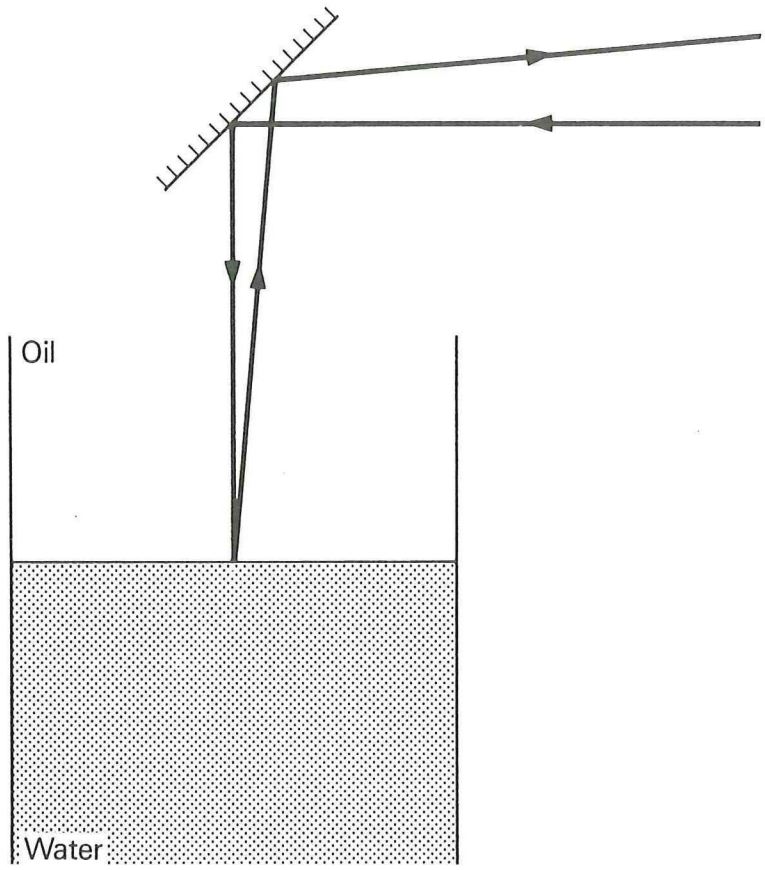

Fig. 4 Perpendicular incidence of the laserbeam

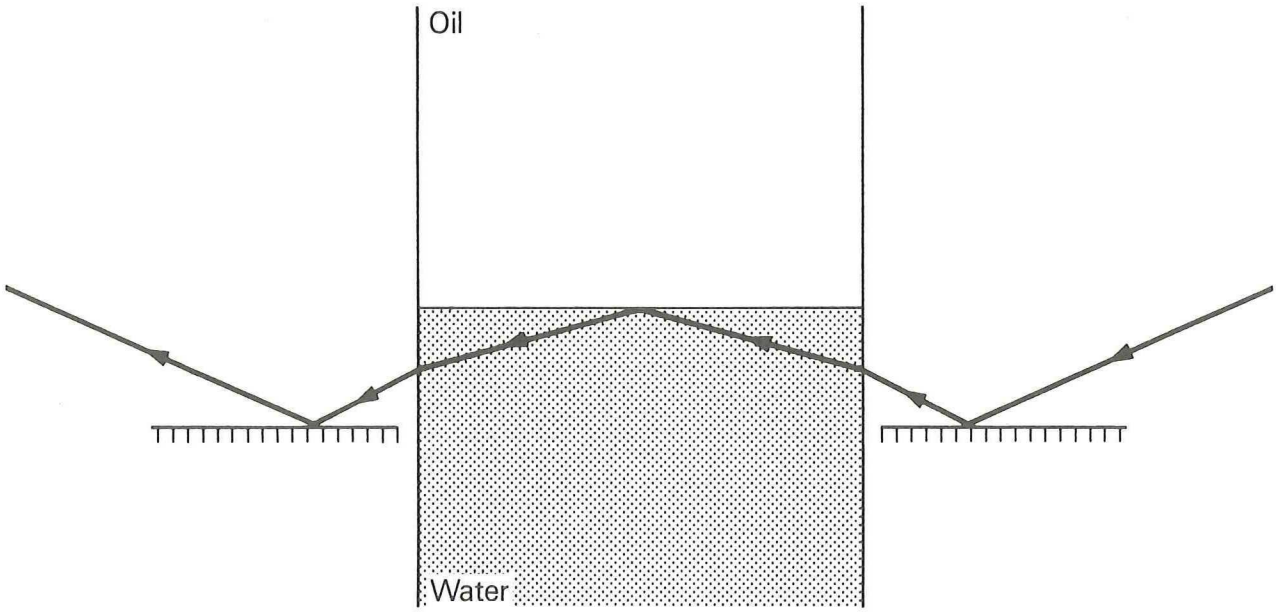

Fig. 5 Grazing incidence of the laserbeam

The different types of detection.

The calculations in this chapter use a simple but accurate representation of the wave by a single frequency sinusoidal wave:

$$z = z_0 \cos(kx-\omega t) \ , \ k = 2\pi/\lambda \qquad (44)$$

A division can be made in six components:
1.)laser. The laser light intensity is modelled by:

$$I = Ae^{-r^2/W^2} \qquad (45)$$

I is the measured intensity, A a constant, r the radius from the centreline and W the radius at which the intensity has decreased by a factor 1/e, here 1mm.
2.)lens. In the focal point of a lens the intensity profile is compressed. W_s the compressed width at the interface can be calculated with the Kogelnik equation:

$$W*W_s*\pi = 4*\lambda^{\ell}*b \qquad (46)$$

λ^{ℓ} is the wavelength of the HeNe-laserlight, 632.8 nm and b the focal length of the lens. this gives a W_s of 48 μm. At the interface a value of 50 μm was measured.

3.)interface. At the interface part of the beam is reflected and part travels through the interface. The waves at the interface modulate the angle of reflection. In figure 6 the effect of different w is sketched. For $W_s << \lambda$ the reflection can be seen as a flat mirror reflection. The direction of the reflected beam will be rotated over twice the angle between the incident beam and the normal of the interface in the plane of the incident beam and the normal.

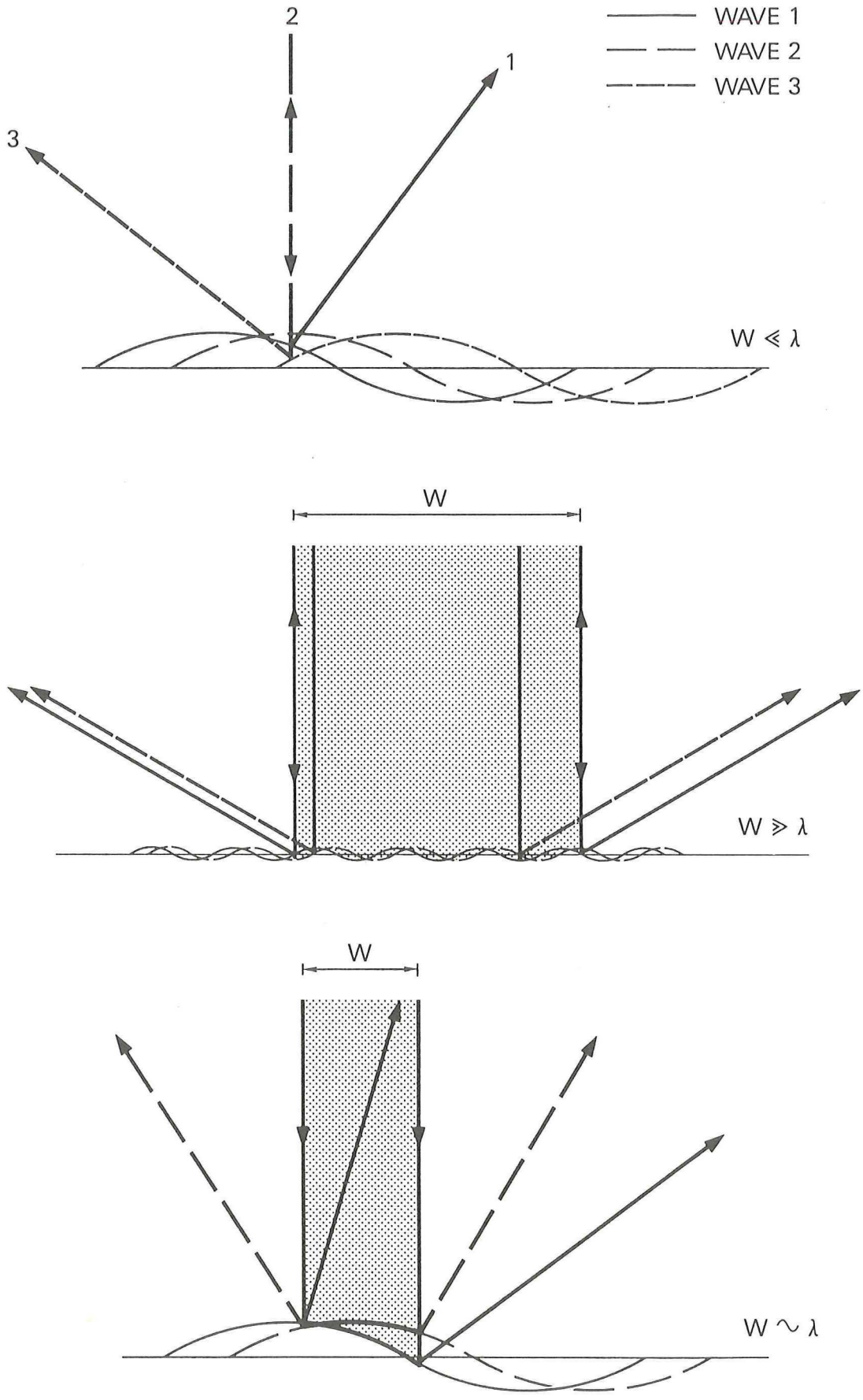

The effect of different beam diameters W ≪ λ (a), W ≫ λ (b), W ∼ λ (c) on the reflection at the interface.

Dr.no. 66742a

FIG. 6

As the angle changes by the progression of the wave, also the direction of the reflected beam changes. The direction of the beam is modulated in time. For $W_s >> \lambda$ the interface acts as a lattice and the reflected light will form a lines or circles pattern. For $W_s \sim \lambda$ the reflection still contains information about the wave. The amplitude of the wave can be derived from the size of the reflected beam.

The region $W_s << \lambda$ is the best to work in, the minimum value for W_s depends on the optical system and can not be lowered much further. To calculate then the intensity profile in the plane of the detector further simplifications are applied:

- reflectivity is constant for small changes in angle.
- the modulation by the wave and the modulation by other sources (like meniscus curvature) are assumed independent and can be superimposed linearly.

4.)detector. At the detector the intensity profile is transformed into a voltage. The voltage is proportional to the center of gravity of the intensity profile. The vertical voltage response $V_e^{d,v}$ of the position sensitive optical detector PSD (two-dimensional position sensing diode) is between +10 and -10 Volts (within 2%) proportional to the vertical displacement δz^d of the centre of the laser beam from the middle of the detector and within ± 5 mm almost independent of horizontal displacement from the middle and over a large dynamical range almost independent of light intensity if stray light is much less intense.

$$V_e^{d,v} \simeq a_e^d \, \delta z^d \qquad (47)$$

where a_e^d is the sensitivity of the detector (approximately 20 V/cm), and δz^d the vertical displacement on the detector

$$\delta z^{d} = b \tan(2\Theta) \simeq 2b\,\Theta = 2b\,\frac{\partial \xi}{\partial x} \qquad (48)$$

where b is the focal length of the focussing lens , and Θ the (small) angle between the vertical and the normal of the interface and x the distance from the centre of symmetry of the wave at the interface

5.)lock-in Amplifier. The voltage from the detector, $V_e^{d,v}$ is then evaluated with the lock-in Amplifier, see appendix 1.

6.) Because of refraction the angle of the laser beam depends on the phase it is traveling through. When a liquid-liquid interface is used the measured interface angle is influenced by this. The calculations can easily be corrected for this effect, see appendix 2.

4 EXPERIMENTS

4.1 Introduction.

The propagation and damping characteristics of capillary waves over fluid/fluid interfaces are determined by the physical parameters of the interface and adjacent phases. The presence of surface active material at the interface influence the wave pattern. Theory gives an expression for the dispersion equation of the waves expressed in bulk and interfacial rheological parameters. Experimentally the waves are induced by the electrical attraction of one bulk phase by a strong localised sinusoidal electrical field from a steel razor blade or needle in the other phase. The blade or needle is positioned a fraction of a millimeter above the interface. The blade leads to a plane wave pattern and the needle to a cylindrical wave pattern. The propagation and damping of the capillary waves is measured by specular reflection of a small laser beam focused on the interface, reflected onto a position-sensitive optical detector. This signal is processed with a lock-in amplifier , information about the phase and magnitude of the wave at a particular point is combined with the dispersion equation to calculate the interfacial properties.

Experiments were carried out with several interface systems:

- water - air
- water - decane - SDS (sodium dodecyl sulphate)
- water - air - stearic acid
- water - Ondina 15 (a mixture of paraffins)
- microemulsions (a mixture of SDS+heptane+butanol+brine)

All these systems have a specific interfacial behaviour. The interfacial tension varies from 0.001 mN/m for microemulsions up to 70 mN/m for water - air. Their dynamic behaviour ranges from simple for water - air to very complicated for water-decane-SDS. The first experiments were performed in a petri-dish. Later on two dedicated measurement cells became available.

4.2 Measurement specifications

In this study several experimental configurations are used. In all cases the slope of the interface is measured as a function of time for different positions with respect to the wave source. This signal can be monitored with a spectrum-analyzer or filtered with a lock-in amplifier.From these measurements we can derive the following interface parameters:

- wavelength λ.
- vertical displacement h(r) of the interface caused by the electrode
- spatial damping coefficient a.

In the first part of the experiments a configuration as given by Ting (9) is used, see page 15. The experimental set up for this configuration is shown in fig 7 and is used to perform scouting experiments with various interface systems to evaluate the method. Two measurement cells have been designed as a follow up from these scouting experiments. They are designed for the use of cylindrical waves with the laser beam grazing the interface. The first cell, Fig 8, will be used to investigate an oil-water system to assess the possibilities of measurements in a pressurised environment. The second cell (Fig 8) will be used to learn more about microemulsion systems.

In these experiments graphs of detector signal spectra and lock-in amplifier output are made. In figures 9, 10 and 11 examples of these graphs are shown. A detailed description of the equipment used is given in appendix 5.

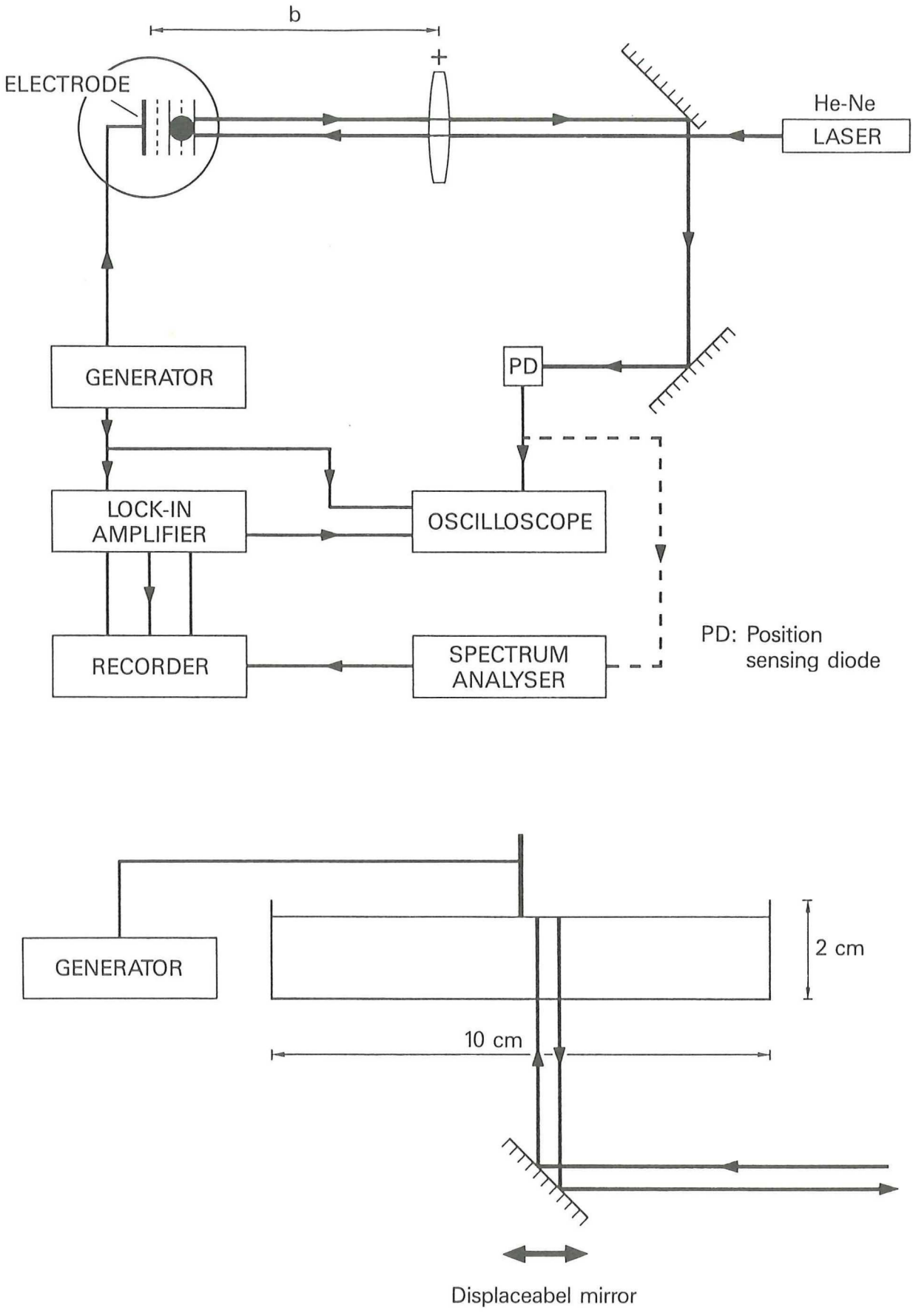

Experimental setup for scouting experiment, top and side view.

Dr.no. 66740a

FIG. 7

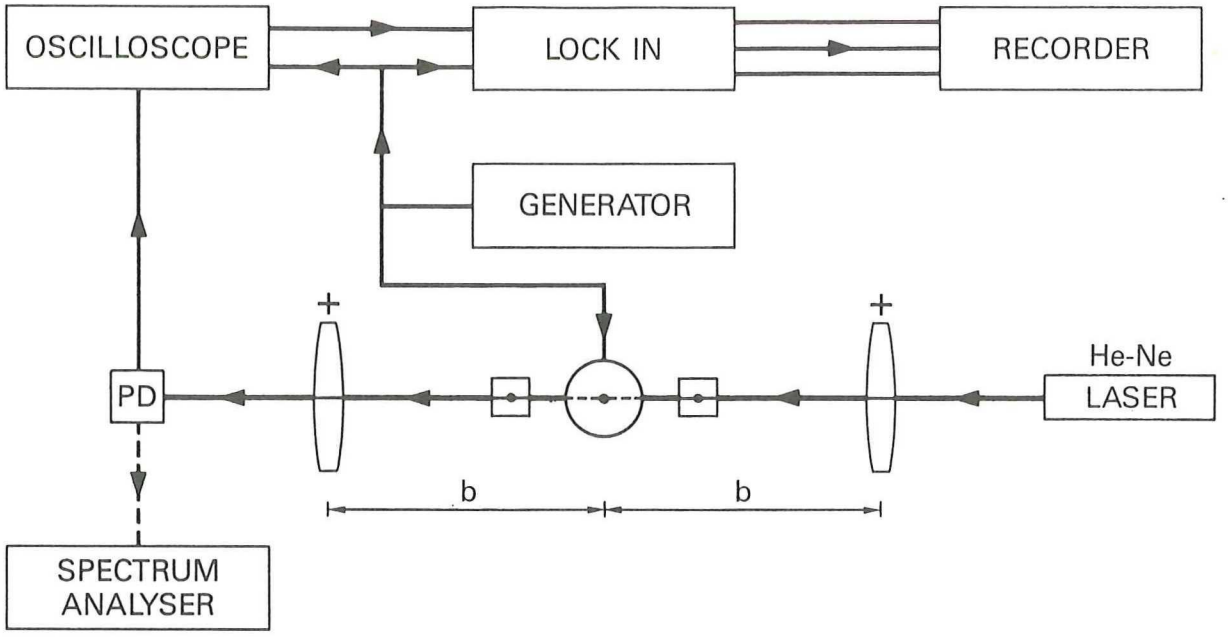

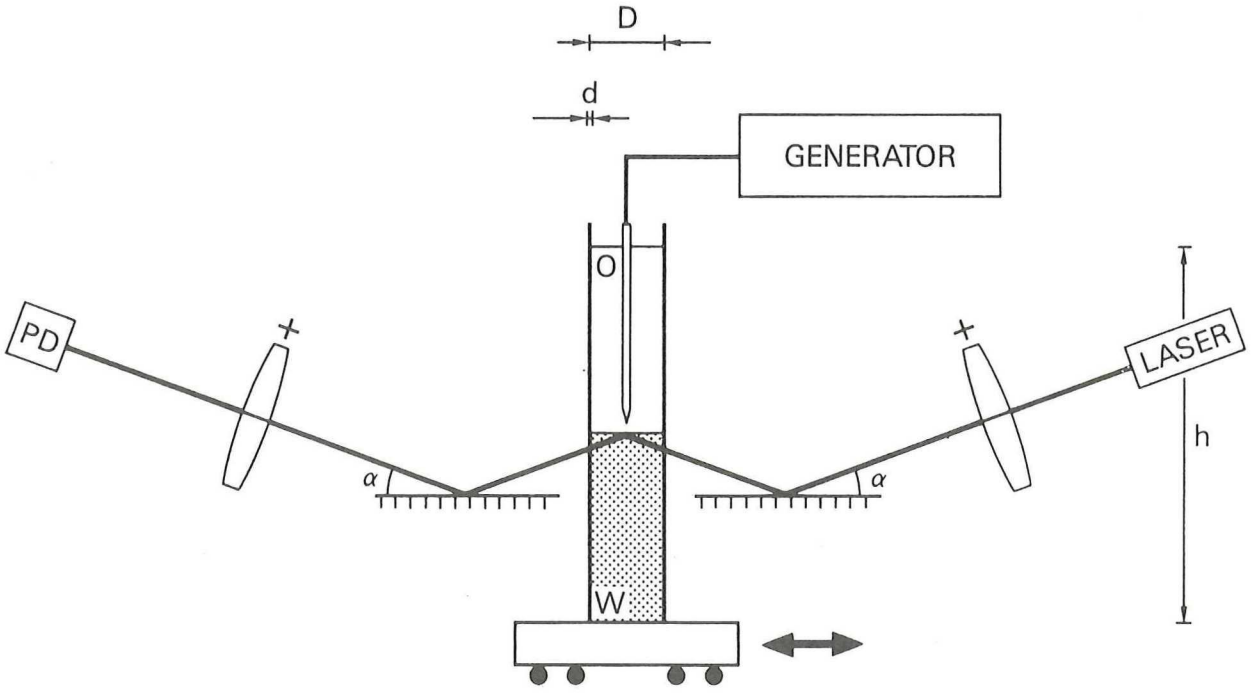

MEASUREMENT CELL	I	D = 19.8 mm h = 100 mm d = 1 mm	II	D = 100 mm h = 100 mm d = 4 mm

Experimental setup for measurement cells.

Dr.no. 66738

FIG. 8

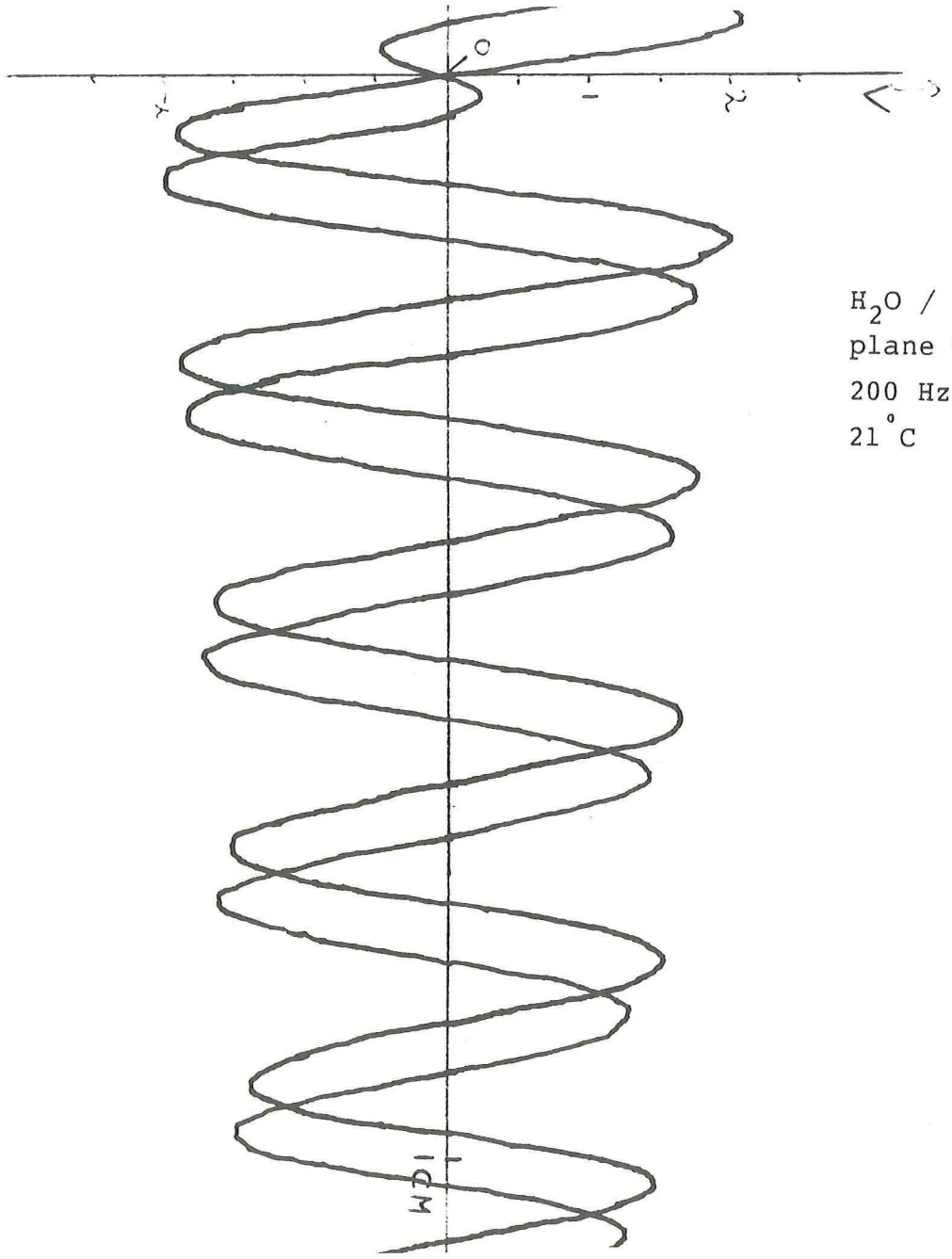

Fig 9. Signal Lock-in amplifier (in phase and quadrature component).

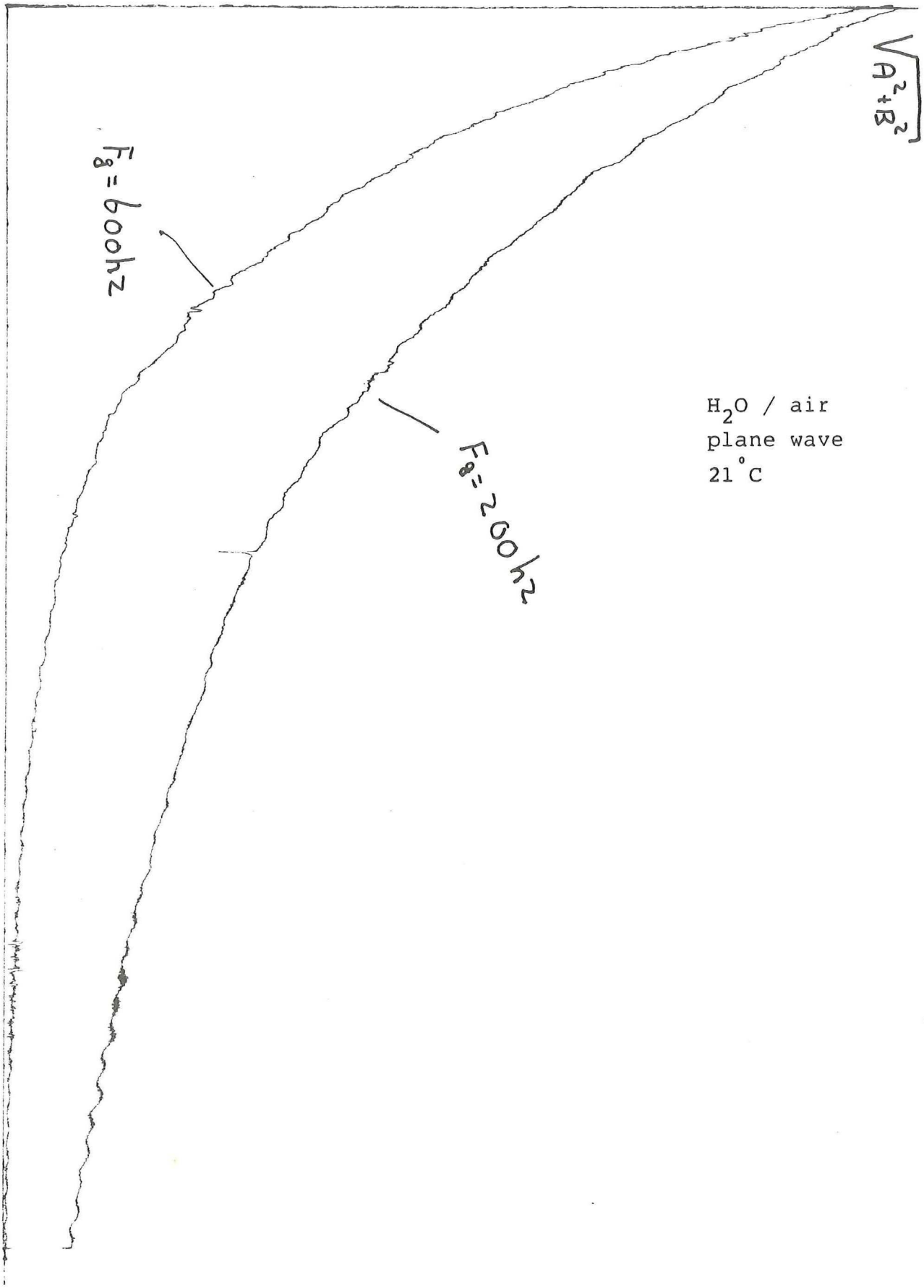

Fig 10 Signal Lock-in amplifier (amplitude) as a function of distance.

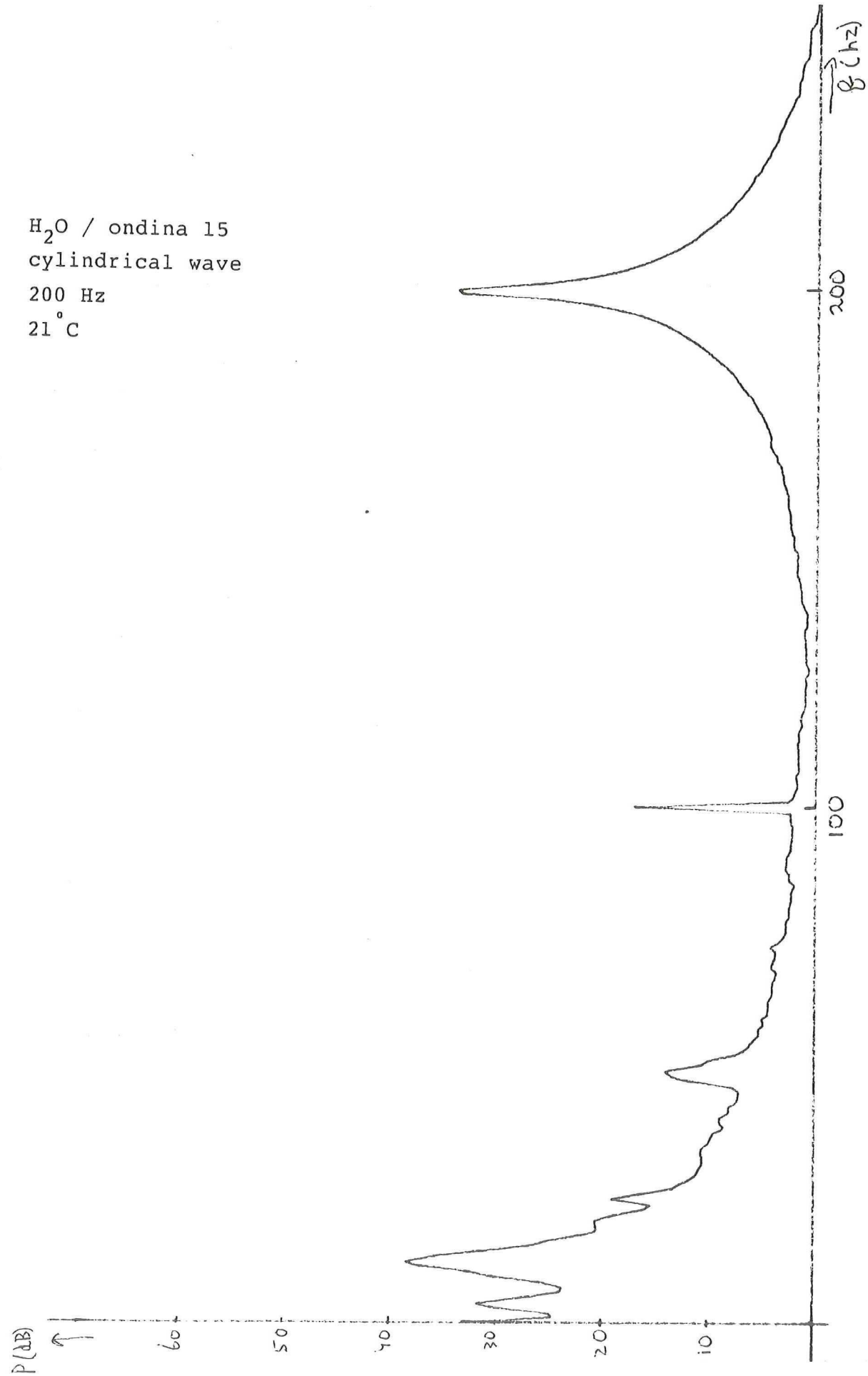

Fig 11. Powerspectrum detector signal (2f)

4.3 Results

4.3.1 Scouting experiments

4.3.1.1 Water - air

It is relatively easy to generate and detect waves in the water - air system. A problem was that the electrode had to be replaced after a few days, due to the corrosion. This problem was solved by coating the blade with an acrylic polymer. The experimental results for this system can be seen in table 1 and figures 12,13 and 14.

Table 1

The distance of interface points with the same phase is measured in a plane wave configuration. The number of wavelengths covered in the measurement is n. From the wavelength λ the interfacial tension γ is calculated using eq. 9. Various wave frequencies f are selected. The damping coefficient a determined from the attenuation over a 20 mm distance. a_t is the theoretical value calculated with eq. 14. The errors $\Delta\lambda$ are estimated by repeating the experiments a few times (over more or different wavelengths) and the corresponding $\Delta\gamma$ are calculated.

f	λ	$\Delta\lambda$	γ	$\Delta\gamma$	n	a	a_t
Hz	10^{-3}m	10^{-6}m	mN/m	mN/m	-	/m	/m
60	5.04	250	66.9	10	5	-	-
120	3.19	100	71.9	7	7	-	-
200	2.253	20	71.5	2	15	-	-
400	1.409	10	70.7	1.6	15	44.3	47.5
600	1.075	5	70.9	1.0	30	-	-
700	0.968	2	70.5	0.4	30	-	-
800	0.886	2	70.6	0.5	30	95.4	95.1
1200	0.675	2	70.5	0.5	40	150.8	142.6

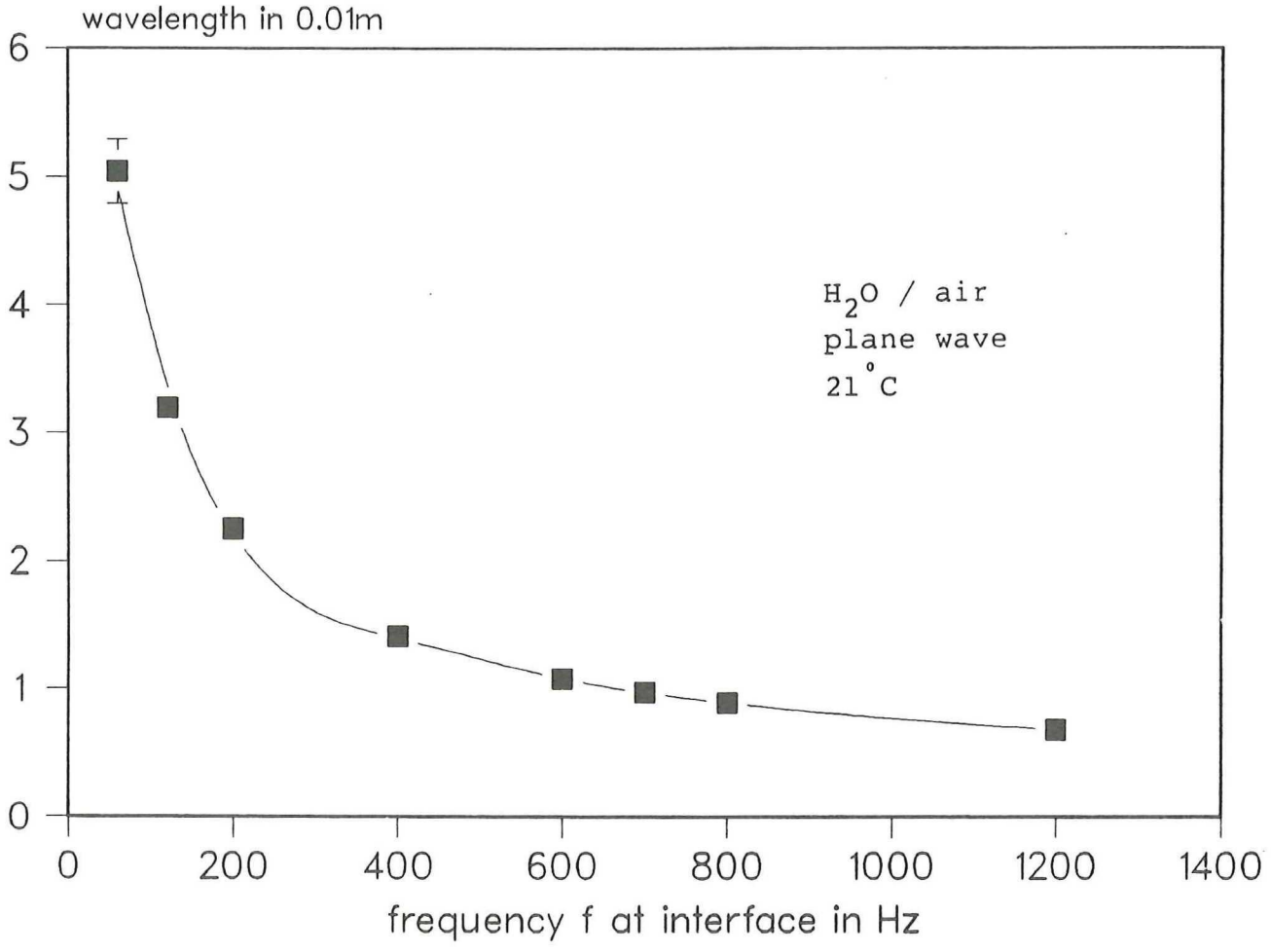

Fig 12. λ the wavelength of the capillary wave at the water -air interface as a function of frequency

γ - f water lucht

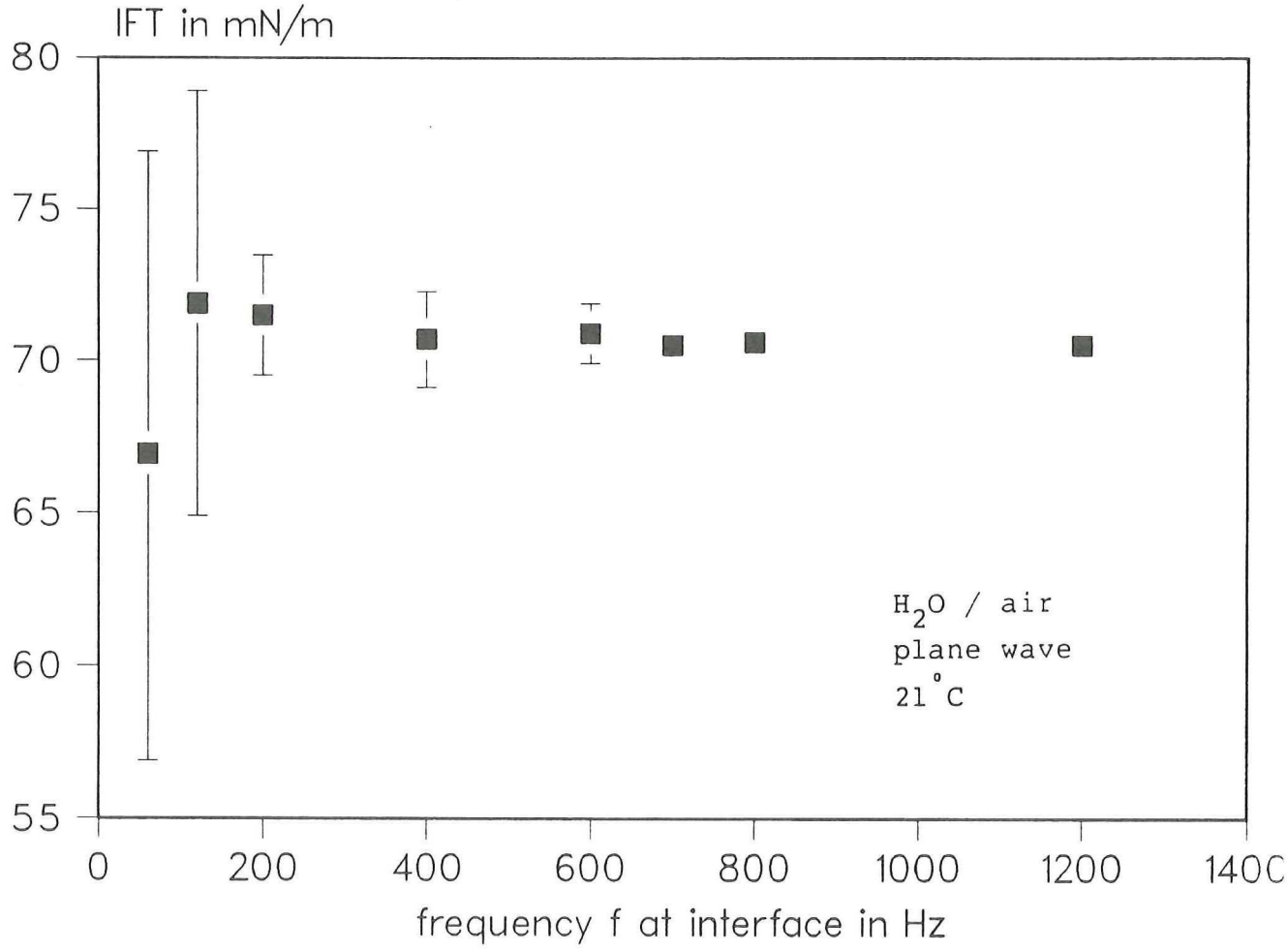

Fig 13. Interfacial tension γ of the water-air interface as a function of frequency.

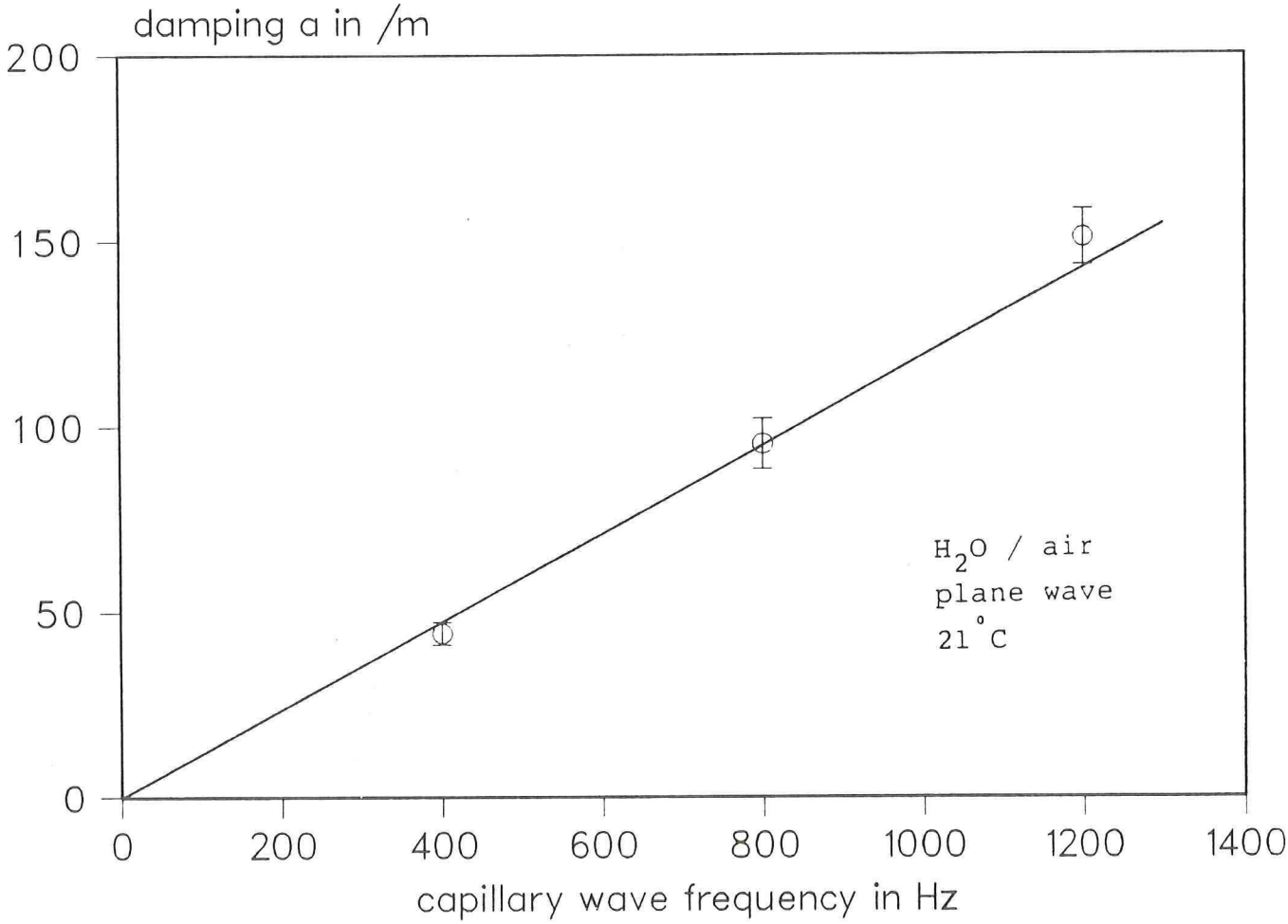

Fig 14. Spatial damping *a* at the water-air interface as a function of frequency.

This table shows that theory and experiments are in reasonable agreement. The values of $\Delta\lambda$ are, for low f ($f \leq 200$ Hz) based on measurements of total distance over n waves and for higher frequencies on reproducibility of the wavelength measurement. The large variation in λ and γ at low frequencies is caused by reflection of the wave at the end of the vessel. This would mean that this effect should dominate at low frequencies, as at low frequencies the damping is small and the wave has still an appreciable amplitude at the end of the vessel. The reflected wave will interfere with the outgoing wave and therefore generate a distorted wave pattern, which gave erroneous results for the λ determination. This interference was shown by measuring the decay of the waves, figure 15. We see in this figure an amplitude variation with distance with two maxima within one wavelength. The amplitude variates over a distance $\lambda/2$. This variation increases due to damping towards the border of the vessel. Another amplitude variation over a distance of approximately 7λ, shows a three times repetition of the long wavelength interference pattern over a radial from electrode to boundary. This might be caused by a slight oblique position of the electrode from the centre of the vessel.

By measuring the dc component of the signal it is possible to calculate the dc-shape of the interface. Without field this gives the (nearly flat) shape of the meniscus in the vessel. With field this shape is distorted near the electrode. The distorsion arises from the average (electrical) attraction of the meniscus by the electrode. Both negative and positive potentials induce attraction. So for a dc field or even for a harmonic field an average attraction or a hump in the meniscus under the electrode is the result. The dc signal is not measured with the lock-in, but with a voltmeter, directly connected to the amplifier of the light signal. The shapes of the measured humps are shown in figure 16.

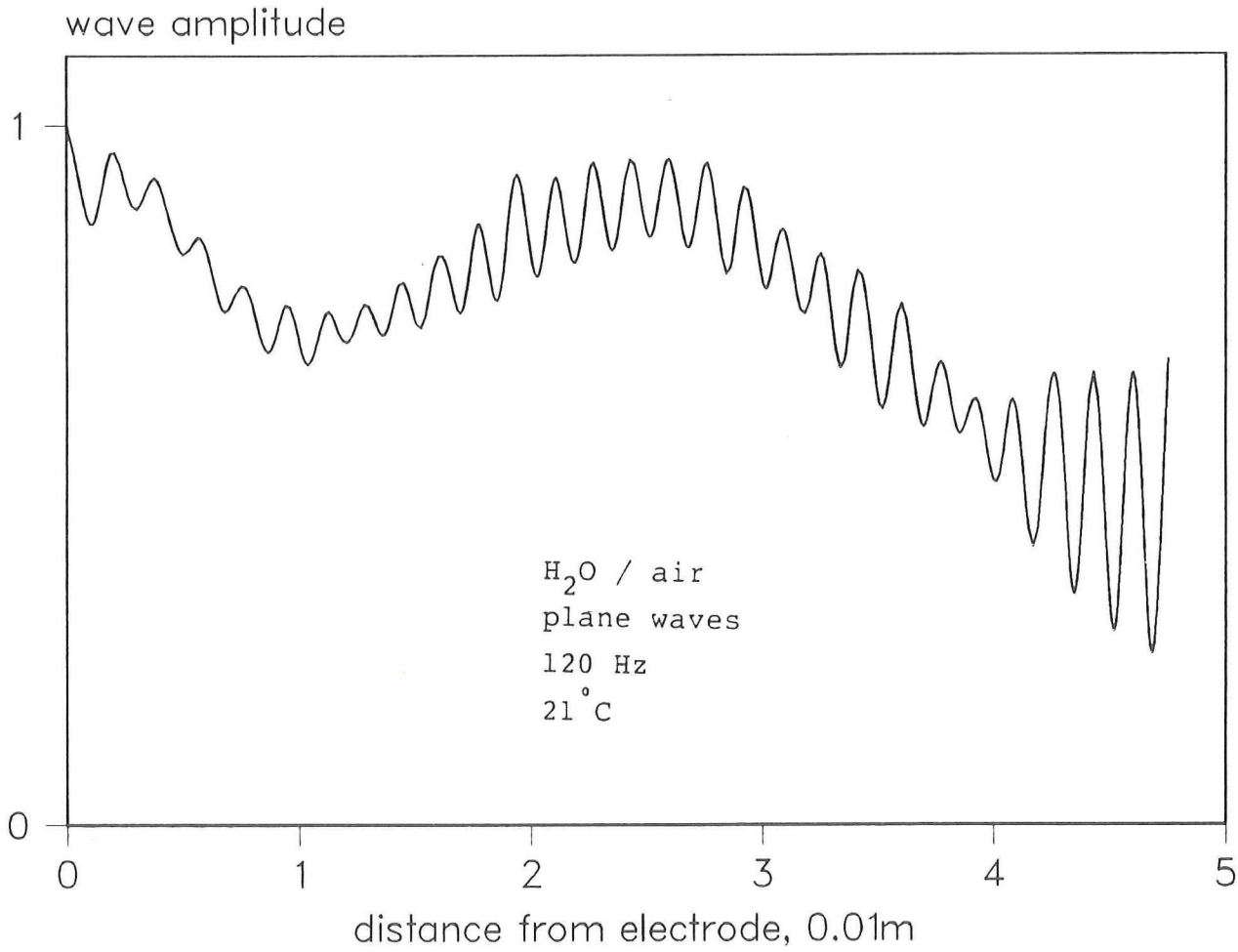

Fig 15. The amplitude variation due to reflection.

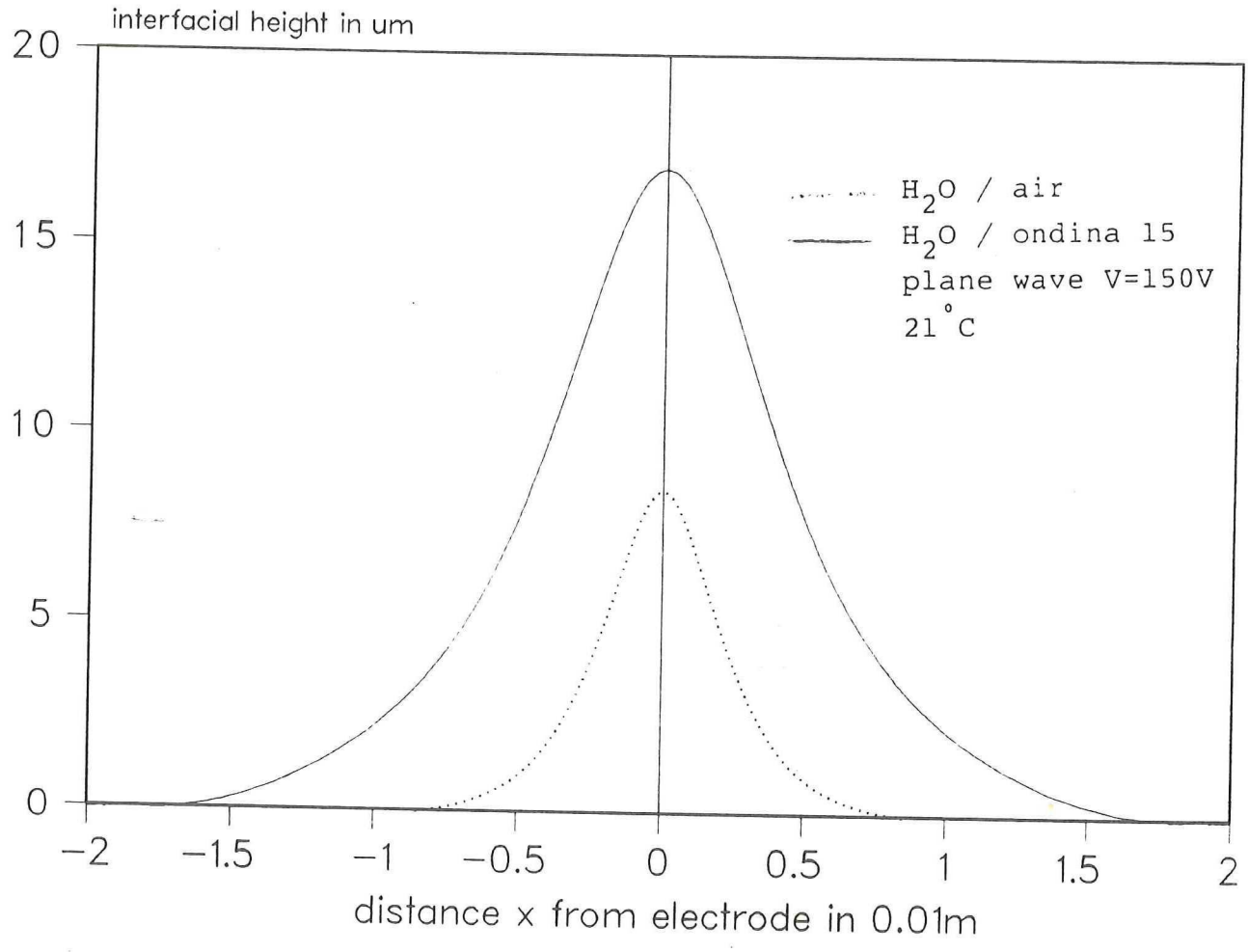

Fig 16. Experimental dc Shape razor blade electrode.

4.3.1.2 (water+SDS) - decane

In this two-liquid system the waves must be generated and detected through one of the liquids. This makes the detection less easy but still possible. The much smaller difference in refractive index causes a much weaker intensity of the reflection at perpendicular incidence of the light and a less intense light signal at the detector. Also the equivalent small $\Delta\epsilon$ gives rise to a lower amplitude/voltage ratio. To prevent electrolysis the electrode must be coated. With the SDS present in this interface system, the measured interfacial tension changes with time. The measured parameters are shown in table 2.

table 2

λ, a and γ as a function of f; n is the number of waves over which is measured, SDS the concentration, a_t is the theoretical damping calculated with eq. 14.

f	λ	SDS	γ	n	a	a/a_t
Hz	10^{-3}m	10^{-6}kmol/m^3	mN/m	-	/m	-
100	2.22	0	29.6	6	-	-
150	1.67	0	28.5	8	-	-
60	-	0.3	-	-	158	1.53
80	1.70	0.3	8.4	5	219	1.59
100	1.45	0.3	8.2	3	-	-
150	1.15	0.3	9.3	4	-	-

The experiments of Ting (Ref.(9)) show a critical micelle concentration CMC of about $1.15*10^{-6}$kmol/m^3 with a corresponding drop in interfacial tension from $\sim$ 22 mN/m to $\sim$ 4 mN/m. In another comparable system, namely water+SDS-air, the commenly reported value of CMC is around $8*10^{-6}$kmol/m^3.

The values of γ shown in table 4 indicate a drop in γ at lower concentration, and therefore a CMC of $0.3\text{-}0.5*10^{-6}$kmol/m^3. The individual values of γ are all somewhat higher than Ting. For the damping Ting (Ref.(9)) found for the ratio $a/a_t \sim 1.5$. This is close to our values found at 60 and 80 Hz.

4.3.1.3 (Water+stearic acid) - air

To introduce stearic acid at the water surface it was dissolved in benzene or toluene. These solvents evaporate quickly of the interface but produce a good spreading of the surfactant. Like SDS, stearic acid is a surfactant, but it is insoluble in water. It forms a monolayer. In many ways it is different from the SDS system.

The density difference in a liquid/gas system between the two bulk phases is much larger than a liquid/liquid system formed by (SDS+water) - decane, leading to a different response. At low stearic acid concentrations the system behaves just like the water - air system. The wave length and therefore the interfacial tension does not vary significantly with the stearic acid concentration even up to high concentrations of the order of a monolayer. However the decay factor a does change with concentration as shown in table 3 and figure 17.

Table 3

The decay factor a and IFT as a function of A, the amount of stearic acid molecules/ unit surface area or B the fraction of surface that is covered by stearic acid (area 1 molecule $\sim 20 \mathring{A}^2$). All these measurements were carried out using a plane capillary wave of 800 hz.

A	B	IFT	a
10^{-9}kmol/m^2	-	mN/m	m^{-1}
0	0	71	95
0.13	0.016	71	95
0.52	0.062	71	100
1.17	0.141	71	150
1.82	0.219	71	290
3.25	0.391	71	230

The damping coefficient a increases above an A value of about $1.2*10^{-9}$; this seems to be the concentration at which the stearic acid molecules begin to repel each other.

4.3.1.4 Water - Ondina 15

Ondina 15 is an oil with a viscosity of 20 cP and a density of 864 kg m^{-3}. The higher the viscosity of one or both bulk phases, the larger the attenuation coefficient a, see eq 14. The high viscosity of the oil phase and thus large a makes it necessary to do measurements at lower frequencies. In table 4 the results for a and γ are shown.

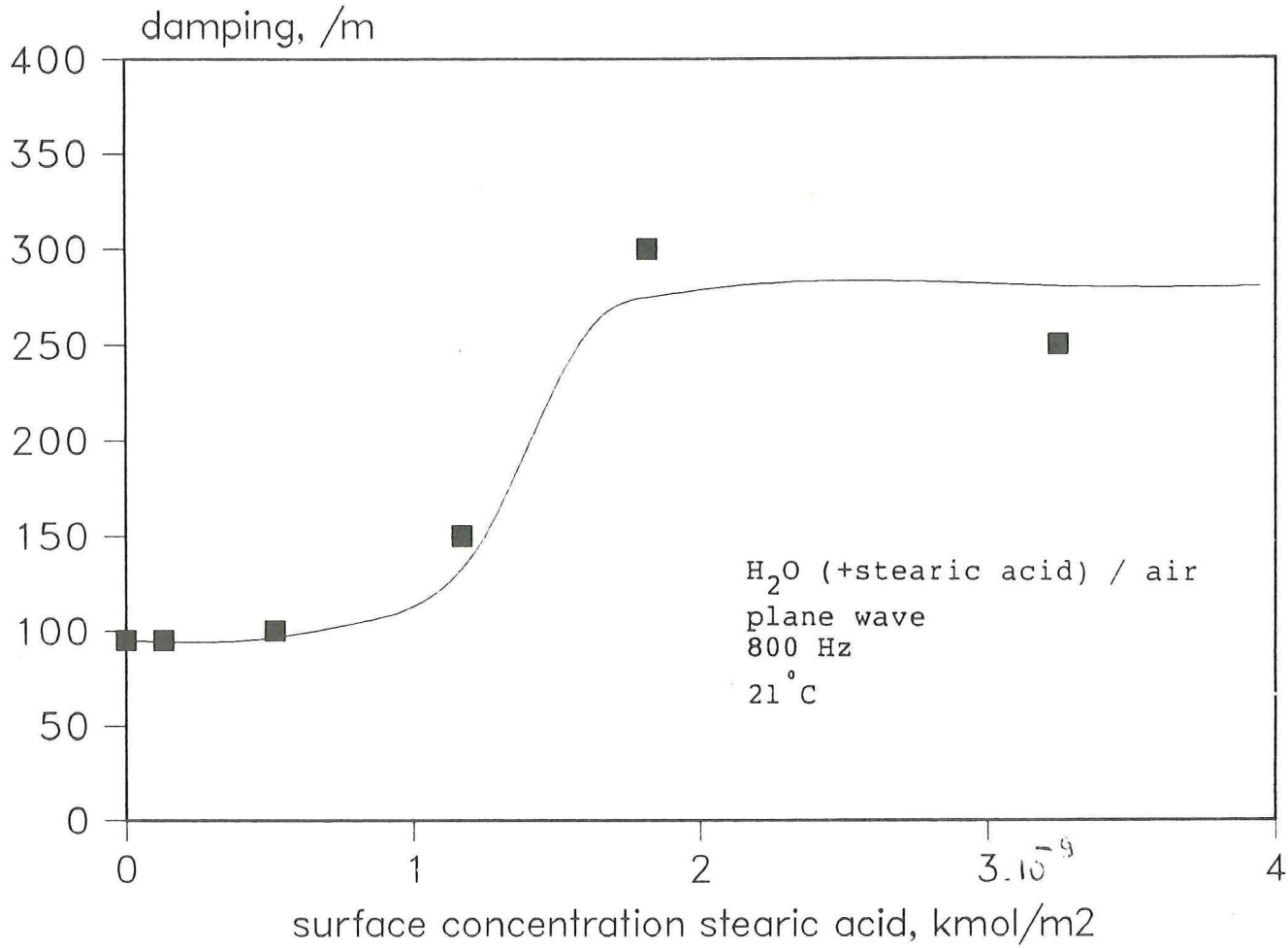

Fig 17. Damping water-air interface surfactant is stearic acid.

Table 4

The results for a and γ for water - Ondina 15. The error for measured a is approximately 5%. γ_t is calculated with eq.9. a_t is calculated with eq.14.

f	a	λ	$\Delta\lambda$	γ	$\Delta\gamma$	γ_t	a_t
Hz	m^{-1}	$10^{-3}m$	$10^{-3}m$	mN/m	mN/m	mN/m	m^{-1}
80	310	2.46	0.01	28.1	0.3	30.5	501
120	459	1.89	0.01	28.7	0.5	30.5	736

The ratio of the measured a and a_t is 0.62.

4.3.1.5 Microemulsions

It is not possible to measure these systems in the configuration used up till now (perpendicular incidence in a Petri dish). This is due to the following problems:

- small Δn, difference in refractive index between the phases. This makes it difficult to detect the reflected laser beam incident at a perpendicular angle with respect to the interface, as its intensity is very low.
- small $\Delta\epsilon$, difference in dielectric constant. This means a small driving force to create waves and a tangential component in the electrical force exerted on the interfase.
- conductivity of two of the three phases, making one interface unreachable.

4.3.1.6 Dynamic behaviour studied by longitudinal waves

The dynamic behaviour was examined for the (water+SDS)-decane and the (water+stearic acid)-air system.

We did use a loudspeaker to induce horizontal oscillatory displacement of a thin wire in an interface. The wire acts like a moving barrier, generating longitudinal waves in the interface. The longitudinal wave produces a local compression of the material at the interface, and a corresponding change in interfacial tension. This change in interfacial tension can then be detected by use of the electrically induced transversal wave, as its wavelength will be modulated. We did prove a modulation in a qualitative way, see figure 18. No quantitative investigation was done. The experimental set up should than be improved to allow quantitative measurement of longitudinal wave amplitude and phase.

4.3.1.7 General problems

Various problems were encountered in the experiments and theoretical developments:

- For microemulsions the refractive index difference between the phases is too small to obtain sufficient reflection of the laser beam, unless a small incident angle is used, smaller than the critical angle.
- The difference in ϵ, the dielectric constant, between both phases can be too small, resulting in a negligible force and thus a wave of negligible amplitude.
- If both fluids have an appreciable conductivity, electrolysis results. This problem was reduced by coating the electrode with an acrylic polymer but this does not improve the field strength.
- The lock-in amplifier showed an offset problem: The zero of one of the signal components was shifted. This produced a periodic distortion in the amplitude signal.

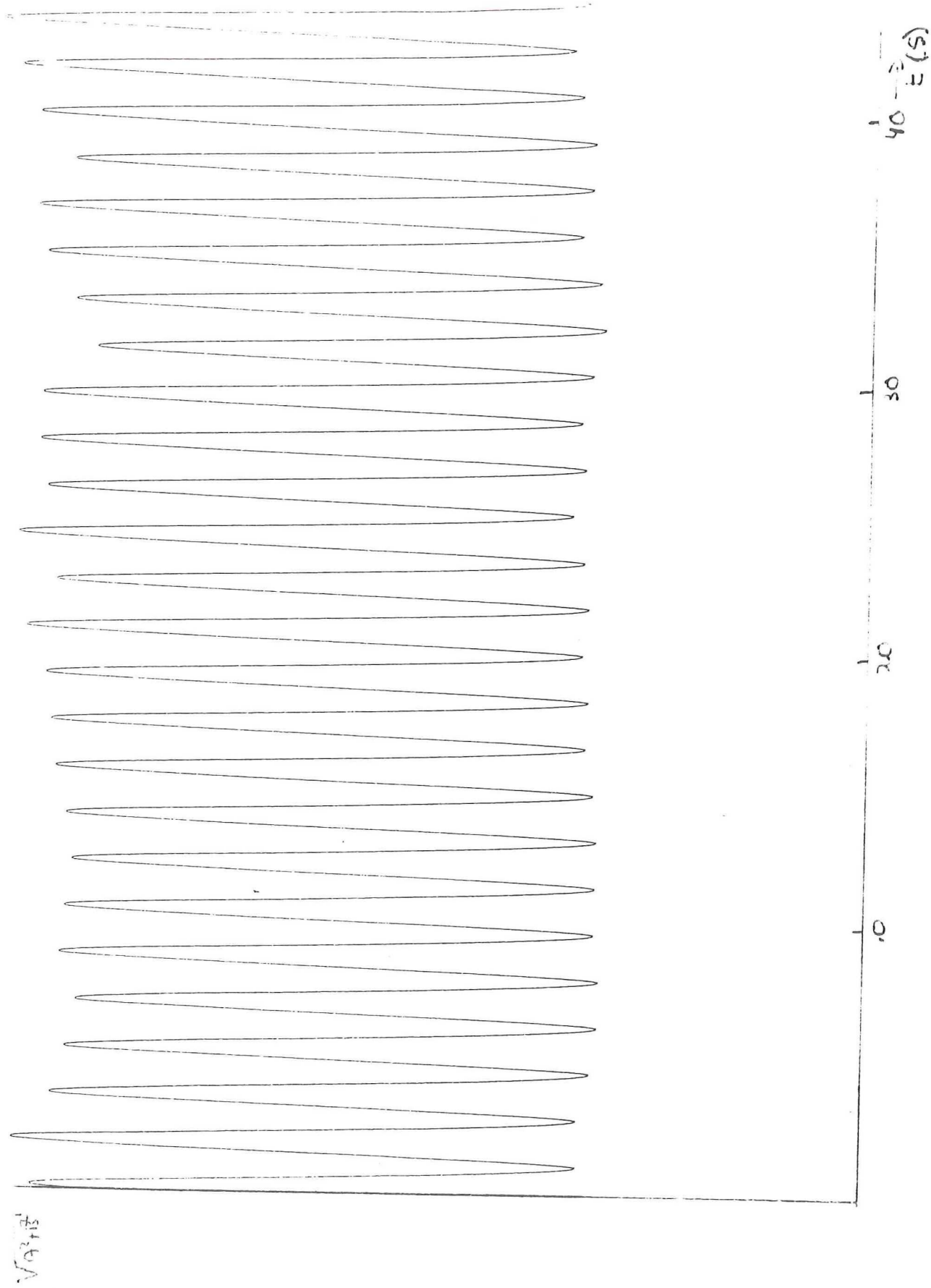

Fig 18. The amplitude of the wave at a given point is monitored against time. Compression and stretching of the interface with a moving barrier leads to variations in a. This can be seen in the amplitude signal as an periodic increase and decrease.

- In testing the optical sensor it became clear that the distance/voltage response was not linear, see appendix 4. We reduced this problem by fixing the average position of the spot in the middle of the detector. We used a servosystem to move the detector, in feedback with the detector output voltage. Because of the slow response of this feedback system, it only fixed the average position of the spot in the middle of the detector. The sluggishness of the servo meant no interference with the ac response (above a few Hz.)
- To measure the wavelength the beam is scanned over the interface. During this scanning the frequency of the signal reaching the lock-in amplifier is changed; while moving in the same direction as the wave apropagates the frequency decreases, while moving in the opposite direction the frequency increases. The lock-in amplifier filters signals with only a response in a small bandwidth, thereby limiting the upper scan velocity of the system.
- The attenuation coefficient a is small at low frequencies, causing reflection of the wave against the boundaries of the vessel, establishing an interference pattern. The magnitude of the introduced error depends on the area of the meniscus.
- The generated waves will be distorted if the electrode is misaligned. This is especially so for the blade electrode.
- Particles, like dust, on the meniscus will adhere to the electrode causing distortion of the field. This problem is also less severe for a needle electrode.
- The limited length dimension of a blade electrode causes end effects. These will interfere with the generated wave at far distances from the electrode.
- Care must be taken to ensure that the laser beam and the mirror stay accurately aligned during movement of the mirror (or equivalently movement of the cell). Small errors (a few percents) are easily introduced in measured radial distance.

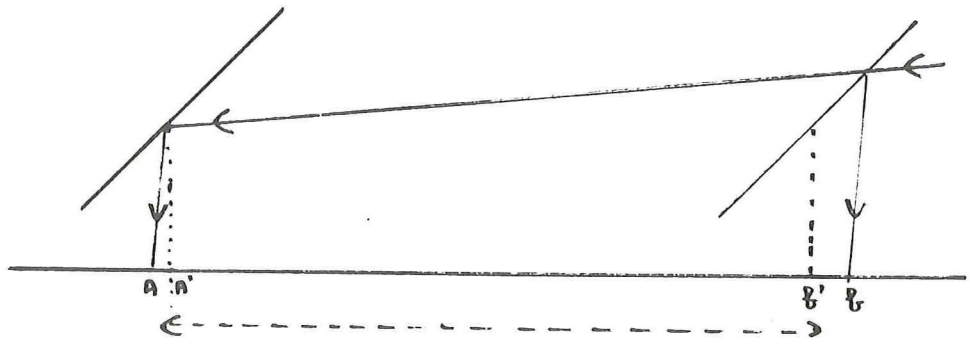

Fig 19. Error introduced when the laser beam and the mirror are not properly alligned.

4.3.2 Measurement cells

4.3.2.1 Introduction

After the above mentioned scouting experiments we built two measurement cells. In both we did use grazing incident laserbeams, but they differed in diameter D, height h, and thickness of the glass.

- D = 19.8 mm , h = 100 mm thickness glass: 1 mm
- D = 100 mm , h = 100 mm thickness glass: 4 mm

The first (smaller) one is used for measurements at an water - Ondina 15 interface. The size of the meniscus in this circular vessel would also be (the maximum size) allowed in pressurised experiments. The small diameter and the height of this vessel made perpendicular incidence of the laser beam rather difficult. This was why also grazing incidence (through the circular side wall) was chosen, although the contrast in refractivity was enough for perpendicular incidence (see §4.3.1.4). With the larger vessel low interfacial tension microemulsion systems are investigated. The microemulsions need grazing incidence of the laserbeam, because of the small difference in refractivity between the phases leading to a decreased intensity of the reflected beam.

4.3.2.2 Measurement cell small geometry

Experiments on such an undersized meniscus gave additional problems.

- flatness of the interface can only be reached by coating the glass and making it partly water-wet and partly oil-wet, see appendix 4
- Extra errors are introduced by the grazing detection. The subsequent refractions over phase-boundaries (including air/glass and glass/liquid) make it difficult to calculate the exact position of the laserspot on the meniscus.
- By measuring the distance of subsequent points of a wave on a radial with a constant phase shift (of 90 degrees) between them, it was detected that these distances varied somewhat, see table 5. Part of this must be associated with the radial symmetry of the wave. A cylindrical wave is described by a function which can be approximated by a single Bessel function. The nodal distances of a Bessel function decrease over a radial. This may explain part (or all) of the observed behaviour. Another effect might be the amplitude of the wave combined with grazing incidence: this might introduce differences in detection of wavecrests and wave-troughs. It was not clear whether the full expression of the wave shape and detection accounts for the overall, somewhat oscillatory, behaviour in nodal distances. Over 360 degrees phase shift the measured oscilation is diminished and the calculated λ seemed to approach the value we expected.

Table 5.

The radial distance Δr and $\Delta r'$ of two points with 90° phase shifts between them at wave frequencies at the interface of 80, 160, and 320 Hz. $\Delta r'$ is the directly measured cell displacement. Δr is the corresponding (calculated and proportional) radial displacement along the meniscus. (water-Ondina 15)

80 hz		160hz		320 hz	
$\Delta r'$	Δr	$\Delta r'$	Δr	$\Delta r'$	Δr
mm	mm	mm	mm	mm	mm
0.405	0.539	0.597	0.794	0.548	0.729
0.679	0.903	0.369	0.491	0.223	0.297
0.505	0.672	0.304	0.404	0.212	0.282
0.483	0.642	0.314	0.418	0.178	0.237
0.487	0.648	0.279	0.371	0.164	0.218
0.454	0.604	0.305	0.406	0.244	0.325
0.440	0.585	0.309	0.411	0.212	0.282
0.504	0.670	0.300	0.399	0.159	0.211
		0.289	0.384	0.166	0.221
		0.274	0.364	0.217	0.289

Based on the distance over last four 90° phase shifts (or last full wavelength), we calculate λ as:

80 hz $\lambda = 2.507$ mm $\gamma = 29.7$ mN/m

160 hz $\lambda = 1.558$ mm $\gamma = 28.6$ mN/m

320 hz $\lambda = 1.003$ mm $\gamma = 30.6$ mN/m

These values are close to the expected value of ~30 mN/m.

Measurements for a were carried out. In table 6 we collect the main results.

Table 6.
Ac-voltage V measured with the lock-in as function of radial distance r for a wave frequency at the interface of 80, 160, and 200 Hz. Also included is a table of the static voltage V(stat) directly measured as the voltage output of the preamplifier. This static component is an indication for the non-zero curvature of the interface. The voltage scaling is different (and not known) in the four cases. (water-Ondina 15)

r' mm	r mm	V(80Hz)	V(160Hz)	V(200Hz)	V(stat)
1.1	1.46	7.75	10.78	7.30	1.45
1.6	2.13	4.85	5.54	3.41	2.11
2.1	2.79	3.15	2.86	1.37	2.77
2.6	3.46	1.94	1.51	0.716	3.43
3.1	4.12	1.39	0.820	0.374	4.09
3.6	4.79	0.992	0.460	0.158	4.75
4.1	5.45	0.608	0.218	0.076	5.41

Offset error in lock-in is 0.001 V
This gives the following values for a:

80 Hz a = 460 /m

160 Hz a = 770 /m

200 Hz a = 950 /m

The static hump h is also measured in this cell see fig 20.

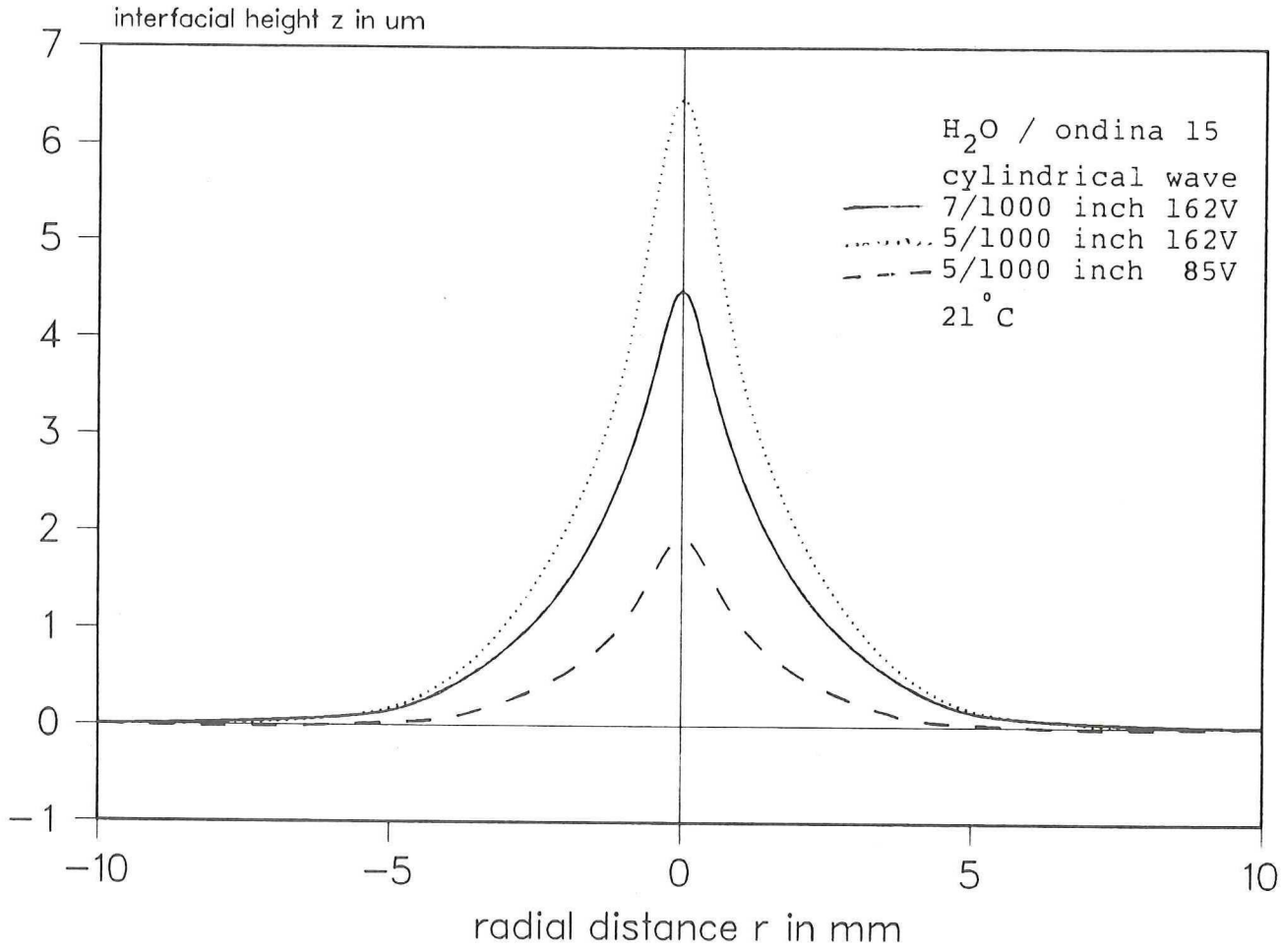

Fig 20. Experimental interface dc shape, needle electrode in small measurement cell with a water-ondina 15 interface.

4.3.2.3 Measurement cell large geometry

The experiments with the microemulsion system gave rise to unexpected phenomena. The interaction between field and interface was very strong. The electrode was used approximately 2 mm above the interface. Instead of the expected 2f signal there was only a wave of frequency f present at the interface. The signal showed no change in phase with respect to the distance from the electrode. The wave was damped within a few mm.

5.DISCUSSION

The scouting experiments indicated that we can determine the interfacial tension with the tranversal wave method. Various interface systems were tested. The measured values for λ and α were in accordance with literature values. It became clear that wavelength measurements are more precise then damping measurements. As a consequence, the interfacial tension can be established with good precision from the wavelength, while other parameters obtained from damping, like viscosity, are less precise. The introduction of a lock-in amplifier improved the signal to noise ratio, but gave also extra experimental problems (Doppler shift, offset). The λ values in the experiments were large enough to neglect the dimension of the laser spot in most experiments, but the ratio of λ and spot dimension determines largely the upper limit of the frequency range. The reflection of waves at the boundary of the interface for low frequencies may cause problems as shown in figure 15. The reflection interference determines the lower limit of the frequency range. Calculation of the interference pattern is difficult and not performed yet, but might prove meaningfull to extend the frequency range. The small amplitude (order μm) compared to the wavelength (order mm), ensures linear behaviour.

The scouting experiments also revealed solvable problems:

- The plane wave generation is sensitive to disturbances, like alignment errors, dust, and limited planar dimension. Cylindrical waves proved to be less sensitive. The larger damping of cylindrical waves proved to be no obstacle.
- Laser reflection at an interface between two fluids of small difference in refraction gave low reflection intensity. In the new measurement cells grazing reflection is used to cope with this problem. Grazing reflection leaded to new problems, like an effective increase of W_s, the effective spot diameter.

  Another problem is the extra uncertainty in where the spot hits the interface, because of additional refractions over boundaries, fig 21.

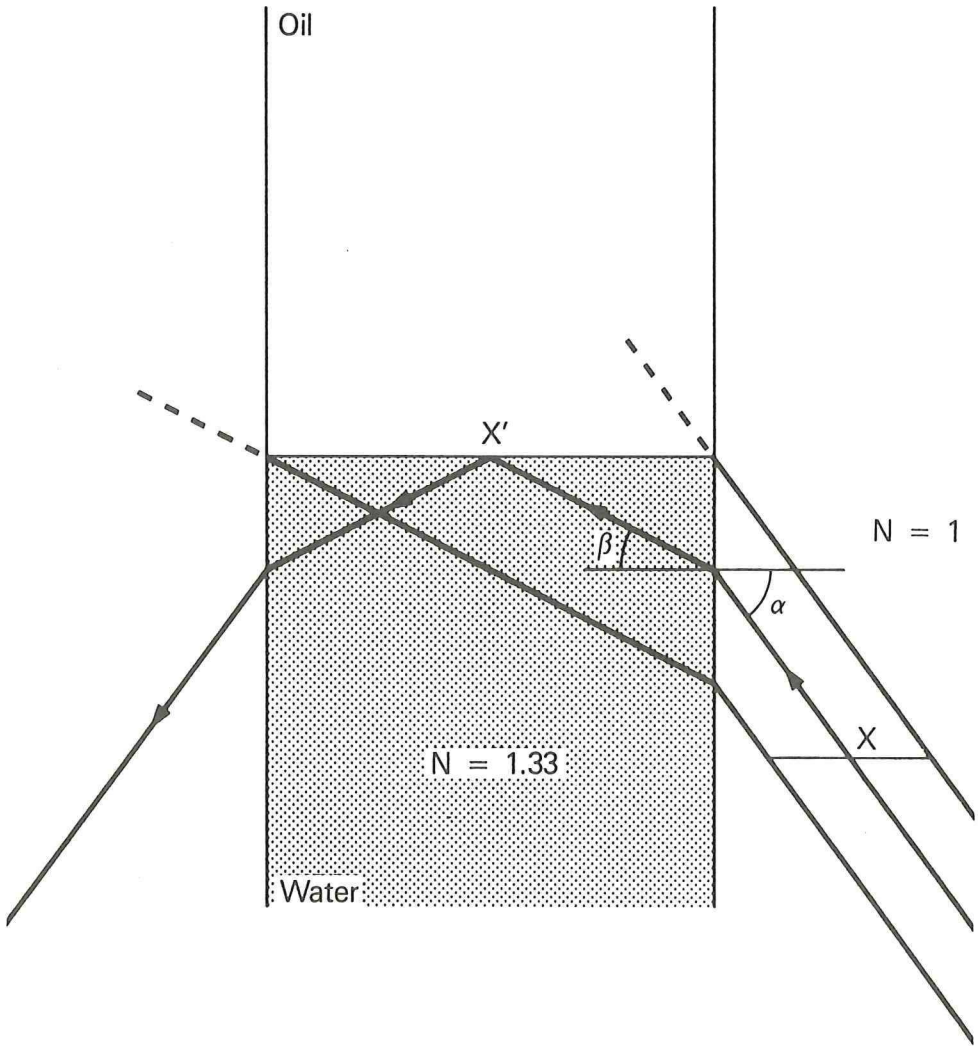

Difference in measurement distance due to refraction.

Later on dedicated measurement cells were designed to do further tests. Eventual pressurisation limits the allowed fluid dimensions, if possible < 2cm and favours circular shape. The experiments show clearly that for an oil-water system this 2 cm is enough to measure interfacial tension accurately (within 1%). In table 5 a phenomenom is showed that only occurred in the small measurement cell, probably this is a mixture of Bessel behaviour (a Bessel function only approaches periodicity for large r) and other alinearities; the resulting λ and γ are close to the expected values.

Microemulsion systems are of interest to SHELL/KSEPL because of their very low interfacial tensions. The scouting experiments showed that microemulsions in the small cell were difficult to measure, because of interface curvature and lack of contrast in refraction between the phases. A larger cell was used. The wave shape over the oil/microemulsion interface seemed very complex, and is not yet fully understood.

The interaction of an interface with an electrical field is accounted for in a simplified theory. The measurement of the static hump compared to calculated ones, see figure 22, showed that the derived theory still needs improvement. Possibly other electrical effects may play a role, f.i. polarization charges influencing γ-values, nonlinearity and higher order interaction of the wave with the field. The hump itself decreases the distance to the electrode and increases the attraction again, etc.

The intention was to study also interfacial rheological parameters, via an additional longitudinal wave imposed on the interface. In some scouting experiments only qualitative results were obtained. It was decided to improve first the IFT determination by tranversal waves before working on dynamics.

The importance of length-measurements, $\gamma \sim \lambda^3_{interface}$, makes it essential to have the distance measurements as precise as possible. Major improvements on accuracy can be made here.

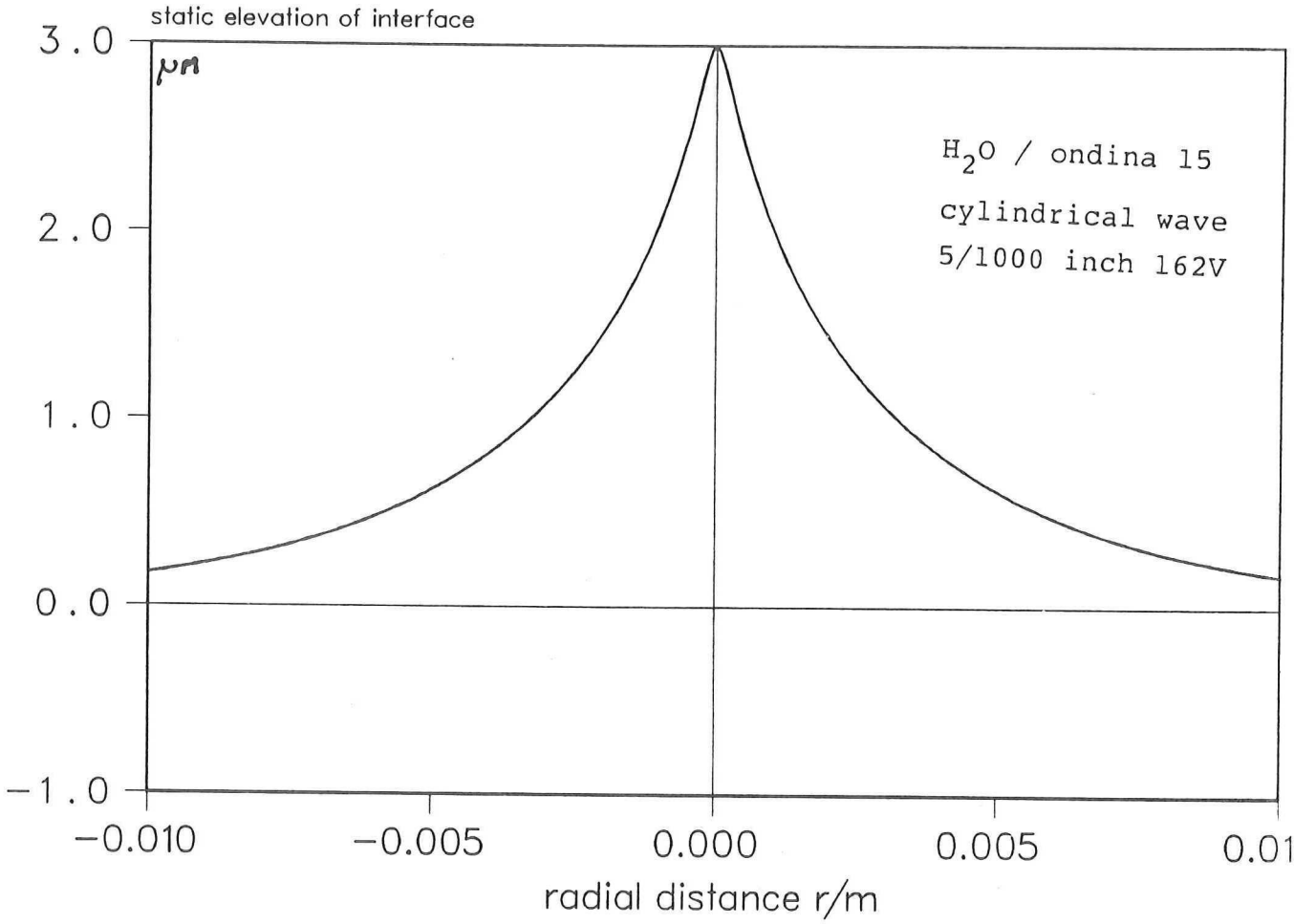

Fig 22. Theoretical interface dc shape, needle electrode in small measurement cell with water/ondina 15.

6 CONCLUSIONS

1) The determination of interfacial tension (IFT) with specular reflection of a small laserbeam with electrically generated propagating capillary waves proves to be possible. As long as the system falls within the following limits:
- One of the phases is non-conducting
- the phases have an appreciable difference in permittivity
- At least one of the phases is transparant for light.

The method is capable to measure IFT with an accuracy smaller then 1%.

2) The IFT is measured from the wavelength of the propagating capillary wave. The damping of the wave can then be used to measure viscosity. However the damping measurements are much less accuarate: the accuracy will be no more then 10% .

3) Dynamical phenomena i.e. changes in interfacial tension with changes in area are made visible. To make quantitative measurements a proper geometry is needed to generate controlable area variations.

4) Measurements with Microemulsion systems could not be done satisfactory. The interaction of the interface (between the oil and microemulsion) with the field was not as expected and further study is necessary to evaluate this.

5) Measurements can be done in a small area of the interface, needed for a pressurised vessel. With a measurement cell (diameter 2 cm) the necessary miniaturisation was investigated. IFT measurements were well possible with this cell.

SYMBOL LIST

a	[m]	height of line charge above interface
$a(k,\omega)$	[m^4s^{-1}]	coef. for ideal term in lower fluid velocity
A	[m^2]	area
b	[m]	focal length of focussing lens
$c(k,\omega)$	[m^4s^{-1}]	coef. for viscous term in lower fluid velocity
CMC	[$molm^{-3}$]	critical mycell concentration
C	[F]	electrical capacity
d	[m]	thickness of the cell glass
d	[m]	diameter of needle
D	[m]	diameter of the measurement cell
D	[m^2s^{-1}]	constant
E_n	[Vm^{-1}]	normal component of electrical field
E_t	[Vm^{-1}]	tangential component of electrical field
e	[-]	2.718281828
$\vec{e}_n$	[-]	normal unit vector
$\vec{e}_\theta$	[-]	unit vector in Cylindrical coordinates
$\vec{e}_r$	[-]	radial unit vector in Cylindrical coordinates
$\vec{e}_t$	[-]	tangential unit vector
$\vec{e}_x$	[-]	Cartesian horizontal unit vector
$\vec{e}_y$	[-]	Cartesian horizontal unit vector
$\vec{e}_z$	[-]	vertical unit vector
F_g	[Nm^{-1}]	gravity potential
f_e^s	[N]	electrical force
f	[s^{-1}]	wave frequency at interface

f_g	[s^{-1}]	generator frequency
$\vec{f}_g$	[N]	gravity force vector
G	[J]	Gibbs free energy
G_x	[N]	external body force
g	[ms^{-2}]	acceleration of free fall
H	[J]	Helmholtz Free energy
h	[m]	height of electrode over interface
h	[m]	heigth of the measurement cell
i	[-]	$i^2=-1$
IFT	[Nm^{-1}]	interfacial tension
Im( )	[-]	imaginary part
J_n	[-]	Bessel function of first kind, order n
K	[m^{-2}]	Gaussian curvature
K_o	[-]	Modified Bessel function of first kind
k	[m^{-1}]	wave number
L	[m]	length
m	[m^{-1}]	wave number real part
ℓ	[m]	length of needle electrode
n	[-]	refraction index
N_e^{li}	[-]	magnification of lock-in amplifier
p,P	[Nm^{-2}]	pressure
p_o	[Nm^{-2}]	
Q	[C]	electrical charge
Re( )	[-]	real part
R_o	[m]	radius
R_1,R_2	[m]	principal radii of curvature of interface
r	[m]	horizontal radial distance

$\vec{r}$	[m]	spatial vector
S	[JK^{-1}]	Entropy
T	[K]	Temperature
t	[s]	time
U	[J]	Internal energy
$\vec{U}$	[m]	fluid particle displacement vector
U_r	[m]	radial fluid particle displacement component
U_z	[m]	vertical fluid particle displacement component
U	[J]	energy
V	[m^3]	Volume
V_e	[V]	electrical potential difference
V_o	[V]	sinusoidal voltage amplitude coefficient
$\vec{V}$	[ms^{-1}]	fluid velocity vector
V_θ	[ms^{-1}]	horizontal Cylindrical fluid velocity component
V_r	[ms^{-1}]	radial fluid velocity component
V_x	[ms^{-1}]	horizontal Cartesian fluid velocity component
V_y	[ms^{-1}]	horizontal Cartesian fluid velocity component
V_z	[ms^{-1}]	vertical fluid velocity component
w	[-]	z=h±wr describes sides of needle electrode for large values of z (z>>h)
W	[m]	1/e intensity radius of a laserbeam
x	[m]	horizontal Cartesian coordinate axis
y	[m]	horizontal Cartesian coordinate axis
Y_n	[-]	Bessel function of second kind, order n
y_n	[-]	general linear combination of Bessel functions
z	[m]	vertical coordinate, elevation above free surface

Greek

a	[m^{-1}]	damping coefficient
a	[rad]	angle of laserbeam
a_e	[Vm^{-1}]	sensitivity of position sensing detector
β	[rad]	angle of the laserbeam
β_e	[Nm^2]	coefficient in electrical force on interface
δ	[-]	Kronecker symbol
δz^d	[m]	vertical displacement of laser spot on diode
$\delta(\ )$	[-]	Dirac delta function
θ	[rad]	Cylindrical coordinate angle
Θ	[-]	tangent of surface: $\partial\xi/\partial r$ or $\partial\xi/\partial x$
$\vec{\nabla}$	[m^{-1}]	gradient operator
Δ	[m^{-2}]	Laplace operator
Δ	[-]	error in the adjacent parameter
ϵ_e	[Fm^{-1}]	permittivity
ϵ_s	[Nm^{-1}]	surface shear elasticity coefficient
ϕ	[rad]	phase angle
γ	[Nm^{-1}]	interfacial tension
ξ	[m]	vertical interface displacement
ξ_o	[m]	stationary component of ξ
κ_s	[Nsm^{-1}]	surface dilatational viscosity coefficient
λ	[m]	wavelength of the capillary wave at the interface
λ^ℓ	[m]	wavelength of the used laser light (HeNe)
λ_s	[Nm^{-1}]	surface dilatational elasticity coefficient
π	[-]	3.141592654
ρ	[kgm^{-3}]	fluid density
ρ_e	[Cm^{-1}]	charge density on needle
Σ	[-]	summation symbol
$\int$	[-]	integration symbol

η	[Pas]	bulk phase shear viscosity coefficient
μ_s	[Nsm^{-1}]	surface shear viscosity coefficient
ω	[s^{-1}]	angular velocity
τ	[s]	integration time of lock-in amplifier

Superscripts

I	[-]	in-phase component
li	[-]	response of lock-in amplifier
Q	[-]	quadrature component
rms	[-]	root mean square
s	[-]	interfacial variable
$\rightarrow$	[-]	vector
'	[-]	prime for upper phase variable

subscripts

ac	[-]	alternating current component
dc	[-]	direct current component
i	[-]	number index; chemical species
n	[-]	integer order of Bessel function
s	[-]	interfacial variable
t	[-]	theoretical value

REFERENCES

1 Herpin, J.C., Meunier, j., J. de Physique, 1974, p.847-859.

2 Cunsolo, S., Jacucci, G., Low Temperature Physics vol 1, 1972, p.337-340.

3 Laboratoire de spectroscopie Hertzienne de l'E., J. de physique, 1971, p.561-571.

4 Hard, S., Neuman, R.D., Journal Of Colloid And Interface Science. 115 1987, p.73-86.

5 Sohl, C.H., Miyano, K., and Ketterson, J.B., Rev. Sci. Instrum. 49, 1978, p. 1464-9.

6 Ting, L., Wasan, T., Miyano, K., J. Colloid and Interface Sci. 107, 1985 p.345-354.

7 Ting, L., Wasan, T., Miyano, K., Xu, S-Q, J. Colloid and Interface Sci. 102, 1984, p.248-59.

8 Miyano, K., Abraham, B.M., Ting, L., Wasan, D.t.,J. Colloid and Interface Sci. 92 1983, p.297-302.

9 Ting, L., Ph.D., thesis, Illinois Institute of Technology, Chicago, III. 1984.

10 Hansen, R.S., and Ahmad, J., "Progress in Surface and Membrane Science" (J.F. Danielli, M.D. Rosenberg, and D.A. Cadenhead, Eds.), Volume 4, p. 1-56. Academic Press, New York, 1971.

11 Mann, J.A.,Jr., Surf. Colloid Sci. 13, 1984, p.145-212.

12 Lucassen-Reynders, E.H., and Lucassen, J., Advan. Colloid Interface Sci. 2, 1969, p.347-95.

13 Scriven, L.E., Chem. Eng. Sci. 12, 1960, p.98-108.

14 Aveyard, R., Haydon, D.A., An introduction to the priciples of surface chemistry, 1973 p.8-18.

15 Jaycock, M.J., Parfitt, G.D., Chemistry of interfaces, 1981, p.22-37.

16 Dorrestein, R., " General linearized theory of the effect of surfacefilms on water ripples. I Proc. K Akad Wetensch. serie B 1951, 54, 260.1

17 Dorrestein, R., " General linearized theory of the effect of surfacefilms on water ripples. II Proc. K Akad Wetensch. serie B 1951, 54, 350.

18 Sohl, C.H., Miyano, K., and Ketterson, J.B., physical review A 22 pp 1256-1265.

19 Kupfmüller, K., "Einführung in die theoretische Elektrotechnik", Chapter 2-I-15, pages 99-101. Springer, Berlin, 1955.

20 Kupfmüller, K., "Einführung in die theoretische Elektrotechnik", Chapter 1-III-9, p. 42-45, Chapter 2-I-13, p. 75-77. Springer, Berlin, 1955.

21 Intern SHELL rapport A.M. Michels

22 Intern SHELL rapport P.B. van der Weg

23 Kelvin, Lord (W.Thomson) Phil.Mag. 42 368.To my regret I did not succeed in obtaining this paper.

APPENDIX 1 Lock-in Amplifier

The reference signal for the lock-in amplifier (Brookdeal, Ortholoc SC 9505) is proportional to the electrical potential on the needle [$\sim\cos(\omega_e t)$]. The lock-in amplifier detects in the 2f-mode only the rms-value of the second harmonic [$\sim\cos(2\omega_e t)$] content of the detected signal $2a_e^d f_1 \partial U_z/\partial r$, thus the harmonic at a frequency $\omega=2\omega_e$. The three channels in the 2f-mode give the in-phase component $V^{li,I}$, the quadrature component $V^{li,Q}$, and the amplitude $V^{li,A}$. A simplified response function for the in-phase component is

$$V^{li,I} \simeq N_e^{li} \sqrt{2} \int_{-\tau/2}^{\tau/2} V_{in} \cos(2\omega_e t) dt \Big/ \int_{-\tau/2}^{\tau/2} dt \qquad (49)$$

where N_e^{li}= 10./(full scale sensitivity/V) is the magnification factor of the amplifier and τ is the integration time of the amplifier. An analogous equation with $\cos(2\omega_e t)$ replaced by $\sin(2\omega_e t)$ gives the quadrature component $V^{li,Q}$. The factor $\sqrt{2}$ is added as the lock-in amplifier gives the rms-value. Thus

$$V^{li,I} = (N_e^{li} 2a_e^d f_1) \frac{\sqrt{2}}{\tau} \int_{-\tau/2}^{\tau/2} (\partial U_z/\partial r)\cos(2\omega_e t) dt \qquad (50)$$

$$V^{li,Q} = (N_e^{li} 2a_e^d f_1) \frac{\sqrt{2}}{\tau} \int_{-\tau/2}^{\tau/2} (\partial U_z/\partial r)\sin(2\omega_e t) dt \qquad (51)$$

$$V^{li,A} = \sqrt{\left[(V^{li,I})^2 + (V^{li,Q})^2 \right]} \qquad (52)$$

APPENDIX 2 Changes in beam angle with phase

Depending on geometry it has the following effect:
1) Perpendicular incident beam.

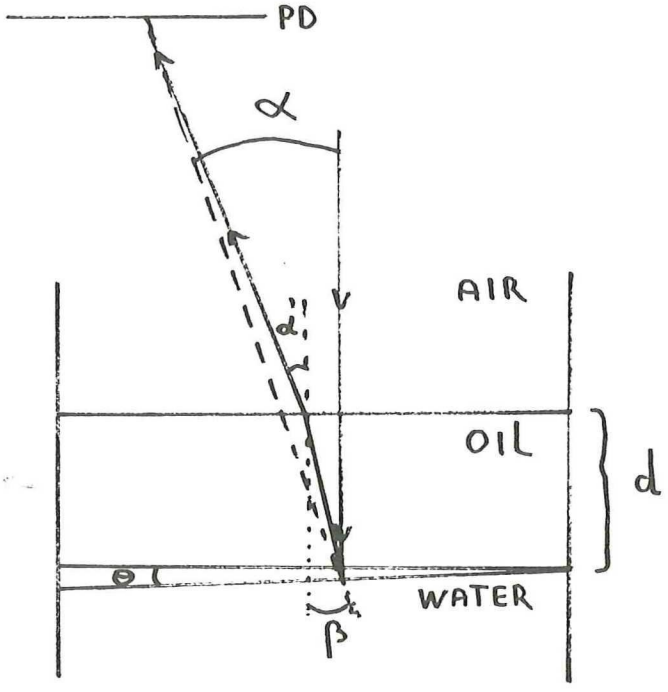

For the angles a and β the following relation holds:

$$n_1 \sin a' = n_2 \sin \beta \qquad (53)$$

Because d the depth of phase 1 is small compared to the focal length of the lens a' equals a and:

$$\sin \beta = \sin a / n_2 \qquad (54)$$

For small a, β sin $(a\beta)$ can be replaced by a, β. This leads to the final expression:

$$\beta = a / n_2 \qquad (55)$$

2) Grazing incidence of the laser beam:

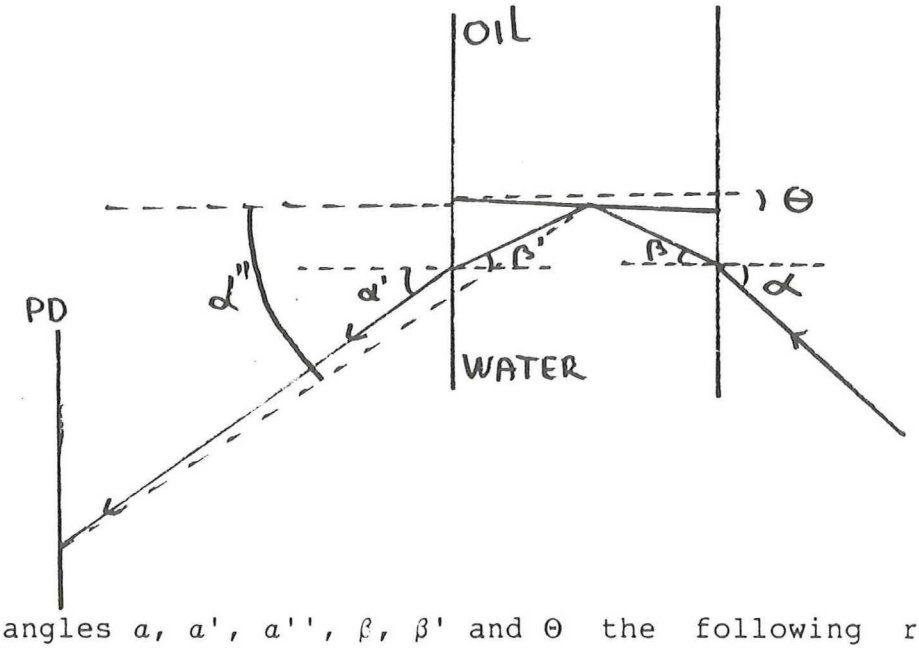

For the angles a, a', a'', β, β' and Θ the following relations hold:

$$1 \sin a = n_2 \sin \beta \qquad (56a)$$

$$1 \sin a' = n_2 \sin \beta' \qquad (56b)$$

$$\beta' = \beta + 2\Theta \qquad (56c)$$

For small D $a'' \simeq a'$ (56d)

With a given a of 21' β becomes 15.6'.

A relation for a' is calculated:

$$\sin a' = n_2 \sin (\beta + 2\Theta) \qquad (57)$$

This expression can be written as:

$$\sin a' = n_2 \sin \beta \cos 2\Theta + n_2 \cos \beta \sin 2\Theta \qquad (58)$$

But $\sin \beta$ is $1/n_2 \sin a$ so:

$$\sin \alpha' = \sin \alpha \cos 2\Theta + n_2 \cos \beta \sin 2\Theta \qquad (58)$$

For Θ small:

$$\cos 2\Theta \simeq 1 \qquad (59a)$$

$$\sin 2\Theta \simeq 2\Theta \qquad (59b)$$

(58)then becomes:

$$\sin \alpha' = \sin \alpha + 2n_2\Theta \cos \beta \qquad (60)$$

α' can be calculated with:

$$\alpha' = \text{arc sin } [\sin \alpha + 2n_2\Theta \cos \beta] \qquad (61)$$

$$\delta z^d = b \tan \alpha'' \quad \text{see (48)} \qquad (62a)$$

$$= b \tan\{ \text{arc sin } [\sin \alpha + 2n_2\Theta \cos \beta]\} \qquad (62b)$$

For the given α and β this leads for small Θ to:

$$\delta z^d = 3.15\ \Theta b \qquad (63)$$

APPENDIX 3 Static humps in small measurement cell

The top angle of the electrode is 21°.
Displacement laserspot see fig 21 can be calculated from the installation angles: (air 21°, water 15.6°) 1.37. It is also possible to measure this displacement directly by moving the table, we measured 1.33.

Table 7. The measurements of the static humps directly measured from the detector. Static means that there is no external voltage and the interface form is dictated by the boundaries.

r'	r	7/1000 inch	Static	5/1000 inch	5/1000 inch
		V=162V	tov X-4	V=162V	V= 85V
mm	mm	V	V	V	V
2.0	2.66	-0.76	-0.40	-1.10	-0.35
1.5	2.0	-1.04	-0.79	-1.50	-0.50
1.0	1.33	-1.60	-1.15	-2.35	-0.72
0.5	0.67	-2.70	-1.45	-4.23	-1.26
0.25	0.33	-3.25	-1.57	-5.44	-1.84
0	0	-1.10	-1.57	-1.96	-0.91
-0.25	-0.33	2.71	-1.22	4.07	1.40
-0.5	-0.67	2.68	-2.05	4.65	1.24
-1.0	-1.33	1.73	-2.76	2.35	0.78
-1.5	-2.00	1.19	-3.06	1.62	0.50
-2.0	-2.66	0.81	-3.20	1.15	0.34
-2.5	-3.33	0.61	-3.27	0.88	0.23
-3.0	-3.99	0.45	-2.80	0.57	0.16
-4.0	-5.32	0.20	0	0.23	0.08

With this table and the formulae from appendix 2 the actual heigth can be calculated. b the focal length was in this case 20 cm.

Table 8. The static hump calculated from table 7 and eqation 3

r	7/1000 inch	STATIC*	5/1000 inch	5/1000 inch
	V=162V		V=162V	V= 85V
mm	µm	µm	µm	µm
5.9	0.08	4.27	0.08	0
4.9	0.16	1.21	0.19	0.03
3.9	0.41	0.09	0.51	0.08
3.4	0.60	0	0.77	0.17
2.9	0.84	0	1.13	0.27
2.4	1.14	0.02	1.57	0.40
1.9	1.54	0.09	2.13	0.57
1.4	2.07	0.23	2.87	0.80
0.9	2.79	0.49	3.92	1.13
0.4	3.78	0.96	5.60	1.62
0	4.50	1.63	6.51	1.99

The other half is symetric for the humps.

APPENDIX 4 Glass preparation for flat interface.

1) First cleaning, use soap and rinse with much water. If the glass is still not visibly clean it can be rinsed with a solution of NaOH in Alcohol.

2) Before etching, rinse with distilled water. The etching is done with a solution of HF in water (we used 5 volume percent). The duration of this etching can be checked by testing the water wetting, if the water wetting is good enough the glass is rinsed with water and dried. Etching must only take place at the glass which will be wet during the experiments, else the glass will be frosted!

3) The glass will now be made completely oil wet. The glass is bathed in dichlor-dimethyl-Silan. A layer of dichlor-dimethyl-Silan is now present on the glass. This makes the glass fully oil wet. To remove the rest of the dichlor-dimethyl-Silan the glass is rinsed with Heptane. The glass is then dried.

4) To make a part of the now perfectly oil wet glass water wet this part is etched again with the HF solution. To get a good result the glass should be etched for approximately 15 seconds and then rinsed with water.

The glass will remain its wetting character at least a few weaks.

APPENDIX 5 USED EQUIPMENT

- Hewlett Packard
  - HP 3582A Spectrum Analyzer
  - HP 3403C True RMS voltmeter
  - HP 7004B x-y recorder
- Kipp en Zonen x-y recorder BD90
- General Radio 1316 oscillator
- displacement monitor(distance→Voltage)
- Tektronics 465B oscilloscope
- Sony
  - magnescale LY-101 + digital gauge DG-100S
- Valy dine SG71 Strain gage amplifier (model MC1-1) (feedback)
- New tronics 200SPC sweep/pulse/function generator
- EG G Brookdeal Ortholoc- SC 9505 Two phase lock-in amplifier
- Oriel Stamford Conn.
  - single controller model 18007
  - Motor Mike 2 inch travel
- Spectra Physics
  - laser exciter 215-2
  - Spectra Physics laser (He-Ne 10mW) 105-1
- BK loudspeaker
- United Detector Technology
  - position sensing diode PIN SC-4D
  - signal conditioning amplifier 301DIV
- Electrodes
  - razor blade
  - needle stainless steel, top angle of 21°
  - needle platinum, top angle 17°
- Optical units
  - flat mirrors
  - displacement tables
  - lenses (Focal length of 20, 30 and 60 cm)
- small dc electromotor to drive the detector feedback

Onder in de conus levert dit een fout op in elongatiesnelheid van maximaal 25 %(dit verklaart de vaak grote spreiding in meetresultaten voor grote deformaties.). Boven in de conus is de fout 4 %.

De fout die gemaakt wordt in Weber is niet alleen van de elongatiesnelheidsfout afhankelijk. Ook de viscositeit, druppeldiameter en grensvlakspanning zijn belangrijk. Van deze drie is de fout in de grensvlakspanning verreweg het belangrijkste. Deze fout is af te schatten op ongeveer 6%.

De deformatie wordt ook beinvloed door de fout die wordt veroorzaakt doordat er ook afschuiving heerst. We gaan er van uit dat de druppel op 1 mm nauwkeurig van het midden geplaatst wordt. De fout in de deformatie die dat oplevert kan geschat worden op 17% wanneer de deformatie door afschuiving en elongatie gesommeerd worden.

Conclusie van deze foutenbeschouwing is dat deformatiemetingen niet erg nauwkeurig zijn. De meetfouten zijn vrijwel steeds afleesfouten. Dit heeft tot gevolg dat de gemaakte fouten geen systematische fouten zijn. De fouten leveren dus een spreiding op in de meetresultaten. De spreiding in de meetresultaten kan steeds met deze fouten verklaard worden.

7 bespreking meetresultaten

7.1 shearthinning vloeistoffen.

De gebruikte Carbopoloplossingen voldoen goed aan de eisen die aan de druppels gesteld zijn. De elasticiteit van de oplossingen was laag en wanneer de afschuifsnelheden niet groter dan 100 s^{-1} of kleiner dan 0.1 s^{-1} zijn, voldoet de viscositeit goed aan een power-law model.

Het viscositeitsbereik van de oplossingen was echter niet groot. De reden hiervoor is dat de oplossingen wanneer ze teveel Carbopol bevatten bij lage afschuifsnelheden een zeer hoge viscositeit of wellicht zelfs een zwichtspanning bezitten. Met deze oplossingen was een grensvlakspanningsmeting met het spinning-drop apparaat niet meer goed mogelijk. Na de meting relaxeert de druppel niet meer terug naar de bolvorm. Het is zeer waarschijnlijk dat tijdens de grensvlakspanningsmeting de druppel ook niet de vorm bereikt die bij de juiste waarde van de grensvlakspanning hoort. Het is niet duidelijk hoe uit spinning-drop metingen van dergelijke vloeistoffen de grensvlakspanning bepaald kan worden. Daarom is in dit onderzoek geen aandacht aan metingen met Carbopoloplossingen met een grotere concentratie Carbopol besteed. Wanneer de grensvlakspanning niet te bepalen is, is een goede vergelijking van gemeten en voorspelde deformatie is niet meer mogelijk.

Ook de relaxatie van de druppels Carbopoloplossing met grote concentraties Carbopol na het inspuiten naar de bolvorm verloopt traag. Omdat de druppelgrootte in de conus kleiner is dan in het spinning-drop apparaat levert dit bij de gebruikte oplossingen geen probleem op. De grensvlakkrachten zijn dan relatief groter dan de visceuze krachten. In de toevoerbuis naar de conus kregen de druppels genoeg tijd om naar een vorm te relaxeren die niet van de bolvorm te onderscheiden is.

Lagere concentraties Carbopol brengen het probleem met zich mee dat de nauwkeurigheid waarmee de viscositeit gemeten kan worden afneemt.

Het bleek niet mogelijk minder visceuze oplossingen te bereiden waarvan de viscositeit goed meetbaar was.
De bereiding van de oplossingen is met de methode zoals in hoofdstuk 5 beschreven na enig oefenen goed te doen. Enige handigheid is wel vereist.
De deformaties van de druppels Carbopoloplossing voldoen goed aan de voorspelling zoals die door het programma Numdef wordt gemaakt. Uit de figuren 6.2 tm 6.6 valt af te leiden dat de voorspelling waarvoor een verhouding van de effectieve afschuifsnelheid binnen de druppel en de elongatiesnelheid buiten de druppel van 3 wordt aangenomen de beste resultaten geeft. De voorspelde deformatie is gelijk aan de gemeten deformatie voor waarden van $\lambda-1$ die veel groter zijn dan 0.4. Deze waarde is de grootste deformatie die volgens Van de Reijden [2] nog goed aan de theorie van Cox [3] voor Newtonse druppels voldoet. In dit onderzoek zijn geen deformaties gevonden die niet goed aan de voorspelling van Numdef voldoen. De maximale deformatie bedraagt ongeveer 2. Het is opmerkelijk dat de Numdef-voorspelling die afgeleid is van de theorie van Cox [ ] zo'n goede deformatie voorspelling geeft voor dergelijk grote deformaties. Het is daarom niet juist te stellen dat de effectieve afschuifsnelheid binnen de druppel blijkbaar 3 maal de elongatiesnelheid buiten de druppel is. Wanneer dit zo zou zijn hadden de Numdef-voorspellingen voor deformaties groter dan 0.4 ook af moeten wijken van de metingen. Er kan wel worden geconcludeerd dat de voorspelling die met Numdef wordt gedaan een goede voorspelling van de deformatie geeft. Een goede verklaring hiervoor is er echter niet.
De voorspelling van de deformatie volgens Numdef gaat uit van de deformatie voor lange tijden zoals die door Cox gegeven wordt voor Newtonse druppels. Wellicht klopt deze veronderstelling niet. Wanneer de deformatie voor lange tijden kleiner is dan voorspeld wordt wanneer we de theorie van Cox gebruiken en een effectieve viscositeit invoeren, zal de gemeten deformatie niet zoals bij Newtonse vloeistoffen te groot zijn. Dit zou de goede overeenstemming tussen theorie en meting kunnen verklaren. Om dit na

te gaan zullen metingen voor stationaire stromingen in het vier-rollen apparaat uitgevoerd moeten worden zoals Schut [12] voor diverse vloeistoffen al gedaan heeft.

7.2 elastische vloeistoffen met constante viscositeit

De tijdens dit onderzoek gemaakte glucose-Separan oplossingen hebben een vrijwel constante viscositeit. De verschillen tussen deze oplossingen en Newtonse vloeistoffen moeten verklaard worden met de elastische eigenschappen van de oplossingen.
De elasticiteit van de elastische vloeistoffen is niet groot. In verhouding tot de schuifspanningen in de vloeistof zijn de eerste normaalspanningsverschillen van de zelfde orde of kleiner.
Een vergelijking van de meetresultaten en de voorspelling zoals voor Newtonse vloeistoffen geldt is niet gemaakt. De voorspelde deformatie is door Numdef berekend. Door de vrijwel constante viscositeit van deze modelvloeistoffen verschillen beide voorspellingen nauwelijks, zodat het niet nodig is om in de figuren 6.7-6.10 beide modellen weer te geven.
Het valt op dat de gemeten deformatie voor deformaties groter dan 0.4 groter is dan de voorspelde waarde. Dit is het zelfde gedrag dat Newtonse druppels vertonen. Alleen de metingen van de meer visceuze vloeistoffen wijken af. De deformatie is veel groter dan voorspeld is voor deze vloeistoffen. De afwijkingen beginnen al bij lage deformaties. Dit moet een gevolg van de elastische eigenschappen van de druppels zijn. Het opvallende is dat de verhouding tussen eerste normaalspanningsverschillen en schuifspanning voor de druppels met de grootste afwijking van de theorie kleiner dan 1 is. Deze verhouding is voor de laag visceuze oplossingen groter, maar de deformatie wijkt niet of nauwelijks van het Newtonse gedrag af. Blijkbaar worden alleen systemen met een hoge waarde van de viscositeitsverhouding p door de elasticiteit beinvloedt.
De geconstateerde afwijking kan in principe twee oorzaken hebben. De eerste mogelijke oorzaak is een onjuiste voorspelling van de deformatie voor lange tijden. Schut [12] heeft deze einddeformatie voor glucose-Separanoplossingen gemeten. Hij kwam tot de conclusie

dat de vloeistoffen zoals ze hier gebruikt zijn (glucose-Separan-oplossingen) geen afwijkend gedrag vertonen in vergelijking met Newtonse druppels. Weliswaar blijkt een te hoge deformatie te worden gemeten, maar dit gebeurde ook voor Newtonse vloeistoffen. De deformatie voor beide systemen was vrijwel gelijk. In vergelijking met de huidige metingen aan elastische vloeistoffen met een constante viscositeit vond Van der Reijden [2] een kleinere afwijking voor Newtonse druppels in een tijdsafhankelijke stroming. Wanneer de afwijkingen, zoals ze in dit onderzoek gevonden zijn, veroorzaakt worden door een verkeerde voorspelling van de deformatie voor lange tijden, dan waren ook voor Newtonse vloeistoffen deze afwijkingen gevonden. Blijkbaar is dit niet de oorzaak. Schut meet immers nauwelijks verschil tussen beide systemen.

De tweede mogelijke oorzaak is een verkeerde voorspelling van de stapresponsie van de druppel. De stapresponsie zoals gegeven in 2.17 voldoet echter zeker niet beter. Uit figuur 2.2 blijkt immers dat de stapresponsie uit deze vergelijking een kleinere deformatie oplevert dan de stapresponsie volgens de Newtonse theorie. Aangezien bij de metingen een te grote deformatie gemeten is kan met dit model de afwijking niet worden verklaard. Er zal naar een andere oorzaak gezocht moeten worden.

De spreiding in de metingen aan de glucose-Separan oplossingen is groter dan de spreiding in de andere metingen. Dit heeft te maken met de zichtbaarheid van de druppel. De brekingsindex van de continue fase is vrijwel gelijk aan de brekingsindex van de glucose oplossingen. Dit heeft tot gevolg dat de druppel minder goed zichtbaar is. Om hier iets tegen te doen is de disperse fase gekleurd. Omdat de druppels erg klein zijn moet de disperse fase sterk gekleurd worden. Hiervoor is de kleurstof Yellow-Sunset gebruikt. Omdat de druppel door de kleuring een andere grensvlakspanning kan krijgen moet de grensvlakspanning gemeten worden met de kleurstof in de oplossing. Dit bracht het probleem met zich mee dat de druppel in het spinning-drop minder goed zichtbaar was. In dit apparaat is de continue fase namelijk de disperse fase zoals die in de conus gebruikt wordt. Wanneer de glucose-oplossing sterk gekleurd wordt is de druppel in het spinning-drop apparaat

niet goed meer zichtbaar. Grensvlakspannings-metingen zijn dan niet meer nauwkeurig te uit te voeren. Er moet een compromis tussen de zichtbaarheid in de conus en de zichtbaarheid in het spinning-drop apparaat gevonden worden.
Van de gebruikte oplossingen is alleen GLU21-8 niet gekleurd. De concentratie water in deze oplossingen was groter dan bij de andere oplossingen. Dit levert een andere brekingsindex op. De druppels waren goed zichtbaar zonder kleuring.

7.3 viscoëlastische vloeistoffen

De viscoëlastische vloeistoffen die gebruikt zijn waren vrij eenvoudig te maken. De vloeistoffen voldeden zowel wat betreft de schuifspanning als het eerste normaalspanningsverschil betreft goed aan een power-law model. Hoewel dit niet noodzakelijk is, is het toch makkelijk wanneer beide spanningen aan het zelfde model voldoen. De vergelijking tussen beide grootheden wordt erdoor vereenvoudigd.
Vergelijking van de meetresultatan met de door Numdef voorspelde waarde maakt duidelijk dat de waargenomen deformaties veel kleiner zijn dat de voorspelde deformaties. De elasticiteit van de vloeistof moet hiervoor verantwoordelijk zijn. De Numdef voorspelling voor nauwelijks elastische Carbopoloplossingen voldoet immers wel aan de metingen.
De viscositeit van de Carbopoloplossingen heeft als functie van de afschuifsnelheid ongeveer dezelfde vorm als de viscositeit van de Separan oplossingen. De macht van de viscositeit is steeds ongeveer -0.7. Het enige verschil tussen beide vloeistoffen is dus het eerste normaalspanningsverschil. Ook de relaxatietijd van de schuifspanning is bij de Carbopoloplossingen waarschijnlijk kleiner. Hierover is geen goede uitspraak te doen omdat de relaxatietijden van de Separanoplossingen al nauwelijks te meten waren. De Carbopoloplossingen hebben een nog kleinere relaxatietijd die met de beschikbare apparatuur niet meer te meten was. Uit het voorgaande kan worden geconcludeerd dat de verschillen tussen de Carbopoloplossingen en de Separanoplossingen voornamelijk het

verschil in elasticiteit betreffen. Weliswaar verschillen de grensvlakspanningen van beide vloeistoffen tov ricinusolie fors, maar alle metingen (de theorie van Cox [3] ook) worden tegen het Weber-getal uitgezet. De enige variabelen zijn het Webergetal en de viscositeitsverhouding p. De verschillen in grensvlakspanning mogen geen verschillende deformatie als functie van Weber opleveren.
De meetresultaten voldoen redelijk aan het model zoals dat in hoofdstuk 2 en 4 beschreven wordt voor elastische vloeistoffen. Omdat de viscositeit van de Separanoplossingen niet constant is, kan geen voorspelling voor tijdsafhankelijke deformaties gemaakt worden met het model met twee tijdconstanten (vergelijking 2.17). De vereenvoudiging zoals in paragraaf 4.3 beschreven, kan wel gemaakt worden. Hoewel de tijdconstante van de schuifspanning niet veel groter is dan de tijdconstante voor de Newtonse deformatie (vergelijking 2.14), is de tijdconstante van de schuifspanningsrelaxatie duidelijk overheersend en vooral bij grotere Weber getallen groter.
Wanneer het vereenvoudigde model voor elastische vloeistoffen wordt vergeleken met de metingen valt een grote overeenkomst op. Vooral voor grotere deformaties, waar de veronderstelling dat de ene tijdconstante ten opzichte van de andere mag worden verwaarloosd het meest gerechtvaardigd is, is de overeenkomst tussen voorspelling en meting groot. In ieder geval kan gesteld worden dat de elastische eigenschappen van de vloeistof in dit geval de deformatie verminderen. Er is echter geen zekerheid hoe de deformatie voor lange tijden van deze vloeistoffen zal zijn. Hiervoor bestaan nog geen modellen. Pas wanneer ook hier goede experimenteel getoetste modellen voor zijn, kan een goed gefundeerde uitspraak over de bruikbaarheid van het model van Schut [13] gedaan worden. Deze eerste resultaten zijn echter bemoedigend.
De rol van de verhouding tussen het eerste normaalspanningsverschil en de afschuifspanning is nog niet duidelijk. Het is fysisch gezien niet waarschijnlijk dat het eerste normaalspanningsverschil geen invloed op de deformatie uitoefend. Ook is het verband tussen relaxatietijd en spanning in de vloeistof niet bekend. Het grote

aantal constitutievergelijkingen toont aan dat een algemeen geldend model hiervoor nog niet is gevonden.

8 Aanbevelingen en conclusies

8.1 conclusies

Het blijkt goed mogelijk de deformatie van niet elastische shearthinning druppels in een tijdsafhankelijke elongatiestroming te beschrijven met een aangepaste versie van de theorie van Cox [3]. Deze aangepaste theorie geldt voor deformaties tot ongeveer 2. Het oorspronkelijke model van Cox geldt tot deformaties die kleiner dan 0.4 zijn. Hierbij wordt aangenomen dat de effectieve afschuifsnelheid in de druppel 3 maal de elongatiesnelheid buiten de druppel is.

De viscositeit van Carbopoloplossingen waar suiker aan is toegevoegd zijn goed te beschrijven met een power-law model. Bovendien is de elasticiteit van deze oplossingen in vergelijking met de elasticiteit van andere polymeeroplossingen zeer laag.

De deformatie van druppels suiker-Separan oplossing met elastische eigenschappen en een vrijwel constante viscositeit is groter dan door de Newtonse theorie van Cox voorspeld. De deformatie van deze druppels is echter ook groter dan voor Newtonse druppels door Van der Reijden [2] is gemeten. Een lage elasticiteit is in staat de deformatie te vergroten.

De Separan-suiker oplossingen hebben een vrijwel constante viscositeit. Het eerste normaalspanningsverschil is eenvoudig aan een power-law model te fitten.

De deformatie van de sterk elastische Separanoplossingen is lager dan door Numdef voor shearthinning vloeistoffen voorspeld wordt. Dit is niet verwonderlijk aangezien de elastische vloeistoffen energie op kunnen slaan. Deze energie kan dan niet meer voor de vergroting van de grensvlakenergie benut worden.

De Separan-oplossingen zijn eenvoudig te maken. Ze voldoen voor zowel de schuifspanningen als de eerste normaalspanningsverschillen aan een power-law model.

Het model zoals door Schut is opgesteld voor elastische vloeistoffen is in staat de deformatie van sterk elastische vloeistoffen te voorspellen wanneer de tijdconstante τ kan worden verwaarloosd tov de elastische tijdconstante τ'.

8.2 aanbevelingen

De deformatie voor vooral elastische vloeistoffen moet zowel stationair als tijdsafhankelijk verder gemeten worden. Dan kan worden nagegaan of het model van Schut [13] toepasbaar is op tijdsafhankelijke stromingen.

Shearthinning vloeistoffen zijn niet getoetst op deformaties voor lange tijden. Dit is wel nodig. Wanneer over de deformatie van de druppels voor lange tijden geen zekerheid bestaat, is niet met zekerheid te zeggen of het in Numdef gebruikte model juist is.

De deformatie van druppels met een lage elasticiteit is niet begrepen. Er moet meer onderzoek verricht worden naar de deformatie voor lange tijden en de tijdsafhankelijke deformatie. Bij voorkeur moeten hiervoor de zelfde vloeistoffen worden gebruikt.

Het verband tussen relaxatietijd en het eerste normaalspanningsverschil moet worden onderzocht. Alleen dan kan duidelijk worden wat de rol van het eerste normaalspanningsverschil bij de deformatie van elastische druppels is.

Om het model van Schut [13] toe te kunnen passen voor elastsche druppels zonder constante viscositeit, moet er een oplossing voor de tijdsafhankelijke deformatie volgens dit model gevonden worden. Niet lineaire signaal- en systeemtechnieken moeten hier toegepast worden. Lineaire tchnieken zijn niet bruikbaar.

Literatuurlijst

1) J.J. Elmendorp
A Study On Polymer Blending Microrheology
proefschrift 1986, T.U. Delft

2)C.Van der Reijden-Stolk en A.Sara
A study on polymer blending microrheology part 3
Pol. Eng. Sci. Vol 26 (1986) no 18 p 1229

3) R.G. Cox
J. Fluid Mech. Vol 37 (1969) p 601

4) G.I. Taylor
Proc. R. Soc. A138,(1932) p 41

5) G.I. Taylor
Proc. R. Soc. A146,(1934) p 501

6) S. Van Heel
Deformatie van elastische bolletjes in instationaire elongatiestroming
vierde-jaars verslag 1986 vakgroep T.M.S. T.U. Delft

7) A.V.Oppenheim, A.S.Willsky and I.T. Young
Signals and Systems
Prentice Hall inc.,New Jersey (1983)

8)H.L. Goldsmith and S.G. Mason
The Microrheology of Dispersions
in "Rheology" by F Eirich
Vol 4, p 85-240
Academic-Press, New-York (1967)

9) R.G. Bakker
afstudeerverslag 1985
vakgroep stromingsleer, T.U.-Delft

10) H.B. Chin and C.D. Han
J.Rheol.,(1979) 23,p557

11) C.D. Han
Rheology in Polymer Processing
Academic Press, New-York (1976)

12) J.Schut
vierde-jaars verslag (1986)
vakgroep Fysische Technologie T.U. Delft

13) J.Schut
afstudeerverslag (1987)
vakgroep Fysische Technologie T.U. Delft

14) P.O. Brunn
J.Fluid.Mech.,V 126 (1983) p 533

15) C. Van der Reijden
to be published

16) J.Happel, H.Brenner
Low Reynolds Number Hydrodynamics
Prentice-Hall Inc., Englewood Cliffs, New-York (1965)

17) M.Roukema
afstudeerverslag 1986
vakgroep Technologie van Macromoleculaire Strukturen
T.U. Delft

18) C. Blom, R.J.J. Jongschaap, J.Mellema
Inleiding in de reologie
Kluwer Technische Boeken B.V. Deventer (1986)

19) Q. Van Voorst Vader
afstudeerverslag 1986
vakgroep Fysische Technologie T.U.Delft

20) J.J. Elmendorp & G.de Vos
Measurement of Interfacial Tensions of Molten Polymer Systems by means of the Spinning Drop Method
Pol. Eng. Sci. (1986) Vol.26 no.6

21) B. Vonnegut
Rev. Sci. Instrum. V 13, 6(1942)

APPENDIX 1

Het computerprogramma NUMDEF

```
10 REM DIT PROGRAMMA PLOT DE DEFORMATIE VAN EEN DRUPPEL IN DE CONUS
ALS FUNCTIE VAN HET WEBERGETAL
20 PLOT=0:GERARD=-1
30 NBR=500:PI=3.141592654#
40 EC=.98
50 SG=.027
60 FI=1.34E-07
70 SI=1:SP=6
80 DIM X(500),Y(500),T(500),D(500),G(500),WE(500),Z(100),DE(100)
90 IF PLOT=1 THEN GOSUB 56000
91 INPUT "INVOER VARIABELEN ??????? (1/0)";IN
100 IF IN=0 THEN 170
110 INPUT "aantal stapjes (VEELVOUD VAN 5!!!) ";NBR
120 INPUT "viscositeit continue fase";EC
130 INPUT "grensvlakspanning is";SG
140 INPUT "volumedebiet";FI
150 INPUT "straal druppeltje";RD
160 INPUT "CONUSHOEK";BE:ALF=(BE/180)*PI:
170 INPUT "visc disp. fase. constante factor";KF
180 INPUT "visc.disp. fase. macht";M
190 INPUT "VERHOUDING ELONGATIE-AFSCHUIF VISCOSITEIT";VEA
200 INPUT "verhouding matrix-druppel elongatie";AMD :C=1
201 INPUT "ZIJN DE PARAMETERS JUIST INGEVOERD?(1/0)?????";C
202 IF C=0 THEN 90
210 GOSUB 50000
220 ZO=.014/TAN(ALF)
230 C3=EC*RD/SG
240
TTO=2*PI*ZO^3*(1+2*COS(ALF))*(SIN(ALF))^2/(9*FI*(1+(COS(ALF))^2))
250 T(1)=TTO-2/((3*.001)/C3) :D(1)=0:WE(1)=0
260 TMAX=TTO*(1-(1-11/14)^3)
270 WMAX=2*C3/(3*(TTO-TMAX))
280 DW=(WMAX)/NBR
290 '
300 '
310 FOR I=2 TO NBR
320 PRINT I
330 WE(I)=DW*(I-1)+.001
340 G(I)=WE(I)/C3
350 T(I)=TTO-2/(3*G(I))
360 ED=VEA*KF*((G(I)*AMD)^M)
370 P=ED/EC
380 DE=(19*P+16)*C3*G(I)/(8*P+8)
390 C2=-20/(19*P*C3)
400 D(I)=D(I-1)+(DE-D(I-1))*(1-EXP((T(I)-T(I-1))*C2))
410 NEXT I
420 '
430 '
440 IF PLOT =1 THEN 490
450 TYPE=1 : AL=0 : YTEXT$="L-1" : XTEXT$="We" :
```

```
460 XO=35 :YO=25 : DX=230 : DY=170 :
470 XI=0 : YI=0 : XA=WE(NBR) : YA=D(NBR) : XD=.1 : YD=.2 :
471 PRINT "GROOTSTE WEBERGETAL";WE(NBR):PRINT "GROOTSTE
DEFORMATIE";D(NBR)
472 PRINT "KIES DE SCHAALDELEN OP DE ASSEN ":BEEP
473 INPUT "SCHAALDEEL X-AS ";XD
474 INPUT "SCHAALDEEL Y-AS ";YD
480 GOSUB 51000
490 FOR I=1 TO (NBR/5)
500 X(I)=WE(I*5)
510 Y(I)=D(I*5)
520 NEXT I
530 LINEPOINT$="LINE":STIFT=1:LTYPE=0:PTYPE=16:PSIZE=2:NBR=NBR/5
540 GOSUB 53000:NBR=NBR*5
560 LPRINT"AANTALSTAPJES ";NBR :LPRINT "CONUSHOEK ";BE
:LPRINT"DEBIET" ;FI:LPRINT "GRENSVLAKSPANNING ";SG
570 LPRINT "VISCOSITEIT CONTINUE FASE ";EC:LPRINT "STRAAL DRUPPEL
";RD:
580 LPRINT "VISCOSITEIT DISPERSE FASE ";KF;"*(G^";M;")"
590 LPRINT"VERHOUDING ELONGATIE AFSCHUIVINGS VISCOSITEIT ";VEA
600 LPRINT "VERHOUDING MATRIX DRUPPEL ELONGATIE ";AMD
610 LPRINT "TIJDCONSTANTE";C2:PRINT "GROOTSTE ELONGATIE ";G(NBR)
620 LPRINT "GROOTSTE WEBERGETAL";WE(NBR):LPRINT "GROOTSTE
DEFORMATIE";D(NBR)
621 PRINT " "
622 PRINT " "
630 INPUT "NOG EEN GRAFIEK?,1/0 ";PLOT
640 IF PLOT =1 THEN 90
650 INPUT "MOETEN ER MEETPUNTEN IN DE FIGUUR GEPLOT WORDEN ????";Q
660 IF Q=0 GOTO 1170
670 INPUT "WELKE FILE MOET GELADEN WORDEN
????";FILE$:GERARD=GERARD+1
680 PRINT "DE FILE ";FILE$," WORDT GELADEN"
690 OPEN "I",20#,FILE$:LINE INPUT #20,INFO$
700 PRINT INFO$:I=1
710 INPUT #20,FI,T,ALF,ST,VCC,VCM,VDC,VDM
720 PRINT FI,T,ALF,ST,VCC,VCM,VDC,VDM
730 IF EOF(20) THEN 770
740 INPUT #20,D(I),Z(I),DE(I):PRINT D(I),Z(I),DE(I)
750 I=I+1
760 GOTO 730
770 CLOSE #20
780 NBR=I-1
790 PI=3.1415926536#:PRINT "CONUSHOEK IS ";ALF
800 ZO=.014/TAN(ALF):CS=COS(ALF):PRINT "ZO = ";ZO
810 K=(3*(1+CS)^2)/(4*CS^2*(1+2*CS)):PRINT "K(COS(ALF))=";K
820 FOR N=1 TO NBR
830 G(N)=K*FI*4/(PI*(.014^2)*ZO*(1-(Z(N)/ZO))^3):PRINT Z(N)
840 WE(N)=G(N)*VCC*G(N)^VCM*(D(N)/2)/SG:PRINT G(N),WE(N)
850 NEXT N
860 PRINT "DE PUNTEN WORDEN NU GEPLOT"
870 LINEPOINT$="POINTS"
880 INPUT "WELKE VORM MOETEN DE PUNTEN HEBBEN (0,1,3,4,11 OF 14
?)";PUNT
```

```
890 PTYPE=PUNT:STIFT=1
900 PSIZE=3
910 FOR N=1 TO NBR
920 X(N)=WE(N)
930 Y(N)=DE(N)
940 NEXT N
950 INPUT "MOET ER INFORMATIE OVER DE PUNTEN IN DE GRAFIEK?";INF
951 INPUT "WELKE INFORMATIE";TEXT$
960 IF INF = 0 GOTO 990
970 X(NBR+1)=XA*.05
980 Y(NBR+1)=YA*.9*(1-GERARD*.05):NBR=NBR+1
990 GOSUB 53000
1100 STIFT=1
1110 X=(XA*.07):Y=YA*.888*(1-GERARD*.05)
1120 HEIGHT=4:SPACE=2
1130 BETA=0
1140 GOSUB 57500
1150 INPUT "NOG EEN BESTAND ????";NG
1160 IF NG=1 GOTO 670
1170 GOSUB 56000
1180 END
```

APPENDIX 2

Het computerprogramma waarmee de deformatiegegevens verwerkt worden.

```
10 CLEAR:DIM L(100):DIM B(100):DIM H(100):DIM DH(100):DIM D(100):DIM
SR(100):DIM DE(100):DIM WE(100):DIM Z(100)
20 PI=3.1415926536#
30 INPUT "ONDER WELKE NAAM MOETEN DE MEETRESULTATEN WORDEN
OPGESLAGEN ?";FILE$
40 PRINT "VOER MEETGEGEVENS IN (alsjeblieft)"
50 INPUT "VOLUMEDEBIET = ";FI:INPUT "TEMPERATUUR = ";T:INPUT
"CONUSHOEK = ";ALF:INPUT "GRENSVLAKSPANNING =
";ST:ALF=ALF/180*PI:CS=COS(ALF)
60 INPUT "CONTINUE FASE STANDAARD RICINUS OLIE ? (1/0)";CON
70 IF CON =1 GOTO 100
80 INPUT "VISCOSITEIT CONTINUE FASE CONSTANTE FACTOR = ";VCC
90 INPUT "VISCOSITEIT CONTINUE FASE MACHT = ";VCM:IF CON=0 THEN 110
100 VCC=10^(-.032098*T+.674):VCM=0:PRINT "VCC = ";VCC
110 INPUT "VISCOSITEIT DISPERSE FASE CONSTANTE FACTOR = ";VDC
120 INPUT "VISCOSITEIT DISPERSE FASE MACHT = ";VDM
121 INPUT "PROCESCONDITIES JUIST INGEVOERD (1/0)";PROC
122 IF PROC =0 GOTO 10
130 PRINT "INVOER MEETGEGEVENS"
140 I=1:NOG=0
150 IF I=1 THEN 180 ELSE 160
160 INPUT "EINDE INVOER ?????(1/0)";NOG
170 IF NOG=1 GOTO 270
171 PRINT " "
180 PRINT "MEETPUNT NUMMER ";I
190 INPUT "LENGTE VAN DE DRUPPEL 1/60 MM ";L(I)
200 INPUT "BREEDTE VAN DE DRUPPEL 1/57 MM ";B(I)
210 INPUT "AFSTAND TOT ONDERZIJDE CONUS";H(I)
220 INPUT "AFSTAND VAN DE DRUPPEL TOT HET MIDDEN VAN DE CAMERA 1/60
MM ";DH(I)
221 PRINT " "
230 A=0:INPUT "INGEVOERDE WAARDE VERBETEREN ????? (1/0)";A
240 IF A=1 THEN 180 ELSE IF A=0 GOTO 250 ELSE SOUND 1000,10:GOTO 230
250 I=I+1
260 GOTO 160
270 I=I-1:FOR N=1 TO I
280 D(N)=((L(N)*B(N)^2)^(1/3)/57982!)
290 DE(N)=(L(N)/60000!)/D(N)-1
300 Z(N)=.011/TAN(ALF)-H(N)/1000-DH(N)/60000!
310 PRINT D(N),Z(N),DE(N),TAN(ALF),ALF
320 NEXT N
330 INPUT "MOETEN ER MEETPUNTEN VERANDERD WORDEN ??";MOET
340 IF MOET=0 GOTO 400
350 INPUT "WELK PUNT MOET VERANDERD WORDEN ????";WELK
360 PRINT "D ";WELK:INPUT "NIEUWE WAARDE";D(WELK)
370 PRINT "Z ";WELK:INPUT "NIEUWE WAARDE";Z(WELK)
380 PRINT "DE";WELK:INPUT "NIEUWE WAARDE";DE(WELK)
390 GOTO 330
400 PRINT "MEETGEGEVENS WORDEN WEGGESCHREVEN IN FILE ";FILE$
```

```
410 INPUT "INFORMATIE BOVEN FILE; ";INFO$
420 OPEN "O",#20,FILE$
430 PRINT #20,INFO$
440 PRINT #20,FI,T,ALF,ST,VCC,VCM,VDC,VDM
450 FOR N=1 TO I
460 PRINT #20,D(N),Z(N),DE(N)
470 NEXT N
480 CLOSE #20
490 PI=3.1415926536#
500 ZO=.014/TAN(ALF)
510 K=(3*(1+CS)^2)/(4*CS^2*(1+2*CS))
520 FOR N=1 TO I
530 SR(N)=K*FI*4/(PI*(.014)^2*ZO*(1-(Z(N)/ZO))^3)
540 NEXT N
550 INPUT "MOET ER EEN TABEL VAN DE FILE GEMAAKT WORDEN ????
(1/0)";MOET
560 IF MOET =0 GOTO 840
570 INPUT "STAAT DE PRINTER INGESCHAKELD (1/0)";PR
580 IF PR=1 GOTO 720
590 PRINT INFO$:PRINT " "
600 PRINT "VISCOSITEIT CONTINUE FASE = ";VCC,"*SR^";VCM
610 PRINT "VISCOSITEIT DISPERSE FASE = ";VDC,"*SR^";VDM
620 PRINT " CONUSHOEK                = ";ALF
630 PRINT "VOLUMEDEBIET              = ";FI
640 PRINT "GRENSVLAKSPANNING         = ";ST
650 PRINT "TEMPERATUUR               = ";T
660 PRINT "                  D            DEF           SR
   WE ":PRINT " "
670 FOR N=1 TO I
680 WE(N)=SR(N)*VCC*SR(N)^VCM*D(N)/(ST*2)
690 PRINT N,D(N),DE(N),SR(N),WE(N)
700 NEXT N
710 IF PR =0 GOTO 840
720 LPRINT INFO$:PRINT " "
730 LPRINT "VISCOSITEIT CONTINUE FASE = ";VCC,"*SR^";VCM
740 LPRINT "VISCOSITEIT DISPERSE FASE = ";VDC,"*SR^";VDM
750 LPRINT " CONUSHOEK                = ";ALF
760 LPRINT "VOLUMEDEBIET              = ";FI
770 LPRINT "GRENSVLAKSPANNING         = ";ST
780 LPRINT "TEMPERATUUR               = ";T
790 LPRINT "                  D            DEF           SR
    WE ":LPRINT " "
800 FOR N=1 TO I
810 WE(N)=SR(N)*VCC*SR(N)^VCM*D(N)/(2*ST)
820 LPRINT N,D(N),DE(N),SR(N),WE(N)
830 NEXT N
840 END
```